© 2014. Published by The Company of Biologists Ltd | Journal of Cell Science (2014) 127, 4927–4939 doi:10.1242/jcs.155861

RESEARCH ARTICLE

A novel interaction between Rab7b and actomyosin reveals a dual role in intracellular transport and cell migration

Marita Borg, Oddmund Bakke* and Cinzia Progida*

ABSTRACT

Rab proteins are small GTPases that regulate transport between the different compartments of the endomembrane system in eukaryotic cells. Here, we show that Rab7b, a Rab that controls the transport between late endosomes and the trans Golgi network, interacts directly with myosin II. We illustrate the functional relevance of this interaction, demonstrating that myosin II mediates the transport of Rab7b endosomes, as Rab7b dynamics are strongly affected after myosin II depletion or inhibition. We also demonstrate that a member of the Rab family regulates actin remodeling and, consequently, influences cell adhesion, polarization and migration. We find the molecular mechanism by which Rab7b influences stress fiber formation – through controlling the activation status of the small GTPase RhoA and therefore influencing myosin light chain phosphorylation. Our findings reveal a newly identified role for Rab proteins outside of their canonical role in intracellular trafficking, identifying Rab7b as a coordinator of cytoskeletal organization.

KEY WORDS: Rab proteins, Rab7b, Endosomes, Actomyosin

INTRODUCTION

A complex intracellular compartmentalization is a distinctive feature of eukaryotic cells. To ensure proper communication through the endomembrane system, the transport between all intracellular compartments has to be tightly controlled. Rab proteins are master regulators of intracellular trafficking, controlling all steps from the formation of vesicles from a donor membrane through to their detachment, transport, tethering and fusion with the acceptor compartment (Stenmark, 2009). They are small GTPases that cycle between an inactive GDP-bound and an active GTP-bound form. When activated, they are recruited on membranes, where they bind effector proteins to fulfill their functions (Stenmark, 2009).

More than 60 different Rabs have been identified in humans, and each of them controls a different step of intracellular transport (Stenmark, 2009). We have recently demonstrated that a new member of this family, Rab7b, regulates transport from late endosomes to the trans Golgi network (TGN) (Progida et al., 2010; Progida et al., 2012). Interestingly, we and other groups have observed previously that Rab7b expression is associated with monocytic and megakaryocytic differentiation (Yang et al., 2004; He et al., 2011; Berg-Larsen et al., 2013) and that Rab7b is able to modulate Toll-like receptor 4 (TLR4) and Toll-like receptor 9 (TLR9) signaling in macrophages (Wang et al., 2007; Yao et al., 2009). However, not much is known regarding the mechanisms by which Rab7b regulates these processes. To obtain more insight into the molecular mechanisms controlled by this small GTPase, we searched for its interacting partners.

In this study, we identify an actin motor, myosin II, as a Rab7b effector by using yeast two-hybrid screening. We confirm biochemically the interaction between myosin II and Rab7b, further proving that it is direct, and show that inhibition of myosin II motor by using small interfering (si)RNAs or chemical inhibitors alters Rab7b dynamics.

Myosin II is an actin-binding protein that contracts and crosslinks actin. The ability of myosin II to form filaments and regulate the actin cytoskeleton is controlled by the phosphorylation state of its light chains. By regulating the remodeling of the actin cytoskeleton, myosin II controls processes that require cellular reshaping and movement, such as cell adhesion, polarization and migration (Amano et al., 1996; Aguilar-Cuenca et al., 2014). Strikingly, we observe that Rab7b is also important for actin organization. Indeed, depletion of Rab7b strongly prevents stress fiber formation and cell adhesion on fibronectin, and delays cell migration, indicating a role for Rab7b in controlling actin remodeling.

As Rab7b depletion decreases the fraction of GTP-bound RhoA and phosphorylated myosin light chain (MLC), we propose that Rab7b regulates actomyosin dynamics by modulating RhoA activation and consequently the phosphorylation of MLC.

In conclusion, in this work, we report the discovery that Rab7b and myosin II interact directly in order to regulate intracellular traffic, and importantly, we provide evidence that a member of the Rab family can also control actin organization.

RESULTS

Rab7b interacts directly with myosin II

We have recently identified the small GTPase Rab7b as a regulator of transport from late endosomes to TGN (Progida et al., 2010; Progida et al., 2012). However, not much is known about the mechanisms used by this small GTPase to perform its function. As Rab proteins require specific effectors to regulate membrane transport (Stenmark, 2009), a yeast two-hybrid screen was performed using Rab7b as bait to find its interacting partners (unpublished data). In this way, the actin motor myosin II was identified as a positive hit.

To confirm the results obtained with the two-hybrid screen, we immunoprecipitated Rab7b in monocyte-derived dendritic cells (MDDCs), which express high levels of endogenous Rab7b (Yang et al., 2004; Progida et al., 2010; Berg-Larsen et al., 2013). Endogenous Rab7b was sufficient to co-immunoprecipitate

Department of Biosciences, Centre for Immune Regulation, University of Oslo, Blindernveien 31, 0371 Oslo, Norway.

*Authors for correspondence (oddmund.bakke@ibv.uio.no; c.a.m.progida@ibv.uio.no)

Received 2 May 2014; Accepted 1 September 2014

Journal of Cell Science (2014) 127, 4927–4939 doi:10.1242/jcs.155861

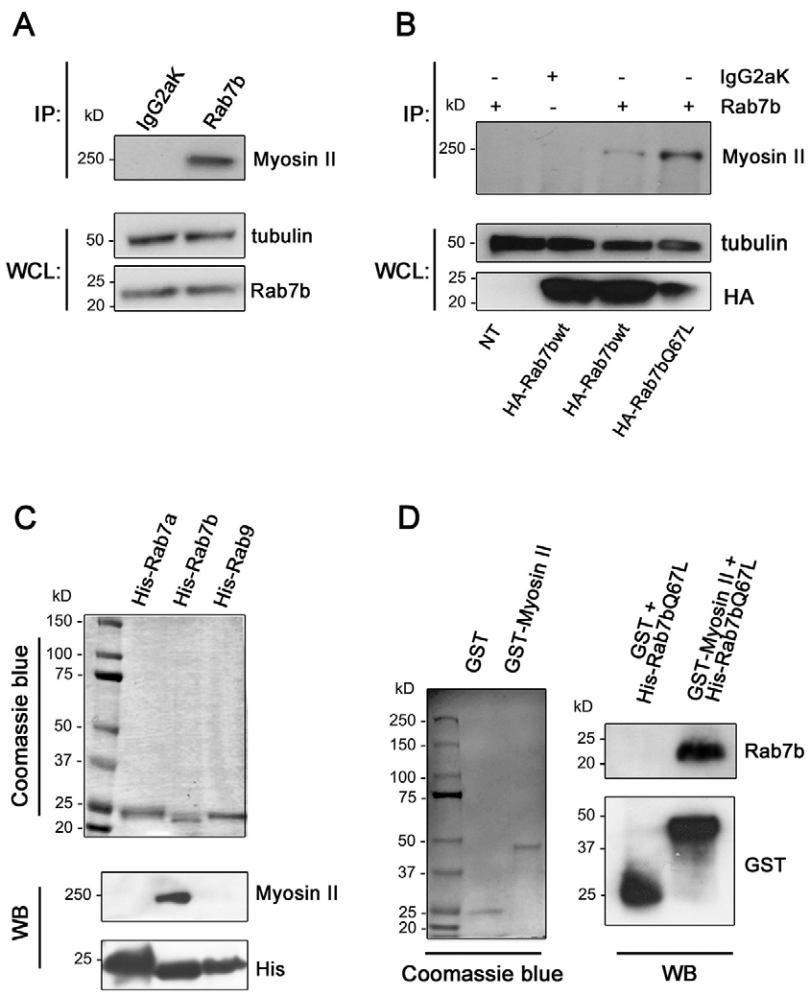

Fig. 1. Rab7b interacts with myosin II. (A) Lysates of monocyte-derived dendritic cells (MDDCs) were subjected to immunoprecipitation with an antibody against Rab7b or an isotype control (IgG2aK). Whole cell lysates (WCL) and immunoprecipitates (IP) were subjected to western blot analysis using antibodies specific to myosin II, tubulin or Rab7b. (B) Lysates of control HeLa cells (NT) or cells expressing HA–Rab7bwt or HA–Rab7bQ67L were subjected to immunoprecipitation with an antibody against Rab7b or an isotype control (IgG2aK). Whole cell lysates and immunoprecipitates were subjected to western blot analysis using antibodies specific to myosin II, tubulin or HA. (C) Upper panel: Coomassie Blue staining of bacterially expressed His–Rab7a, His–Rab7b and His–Rab9 purified using cobalt-coated Dynabeads. Lower panel: bacterially expressed and purified His–Rab7a, His–Rab7b or His–Rab9 were loaded with GTPγS and incubated with lysates from HeLa cells. Proteins were pulled down using cobalt-coated Dynabeads and subjected to western blot (WB) analysis using antibodies against His and myosin II. (D) Left panel: Coomassie Blue staining of bacterially expressed GST and GST–myosin-II-tail purified using glutathione resin. Right panel: purified GST or GST–myosin-I-tail was incubated with purified His–Rab7bQ67L. Samples were subjected to affinity chromatography followed by western blot analysis using antibodies specific to GST and Rab7b.

myosin II (Fig. 1A), thus confirming the authenticity of the interaction.

Next, we transfected HeLa cells with hemagglutinin (HA)-tagged wild-type Rab7b (Rab7bwt) or the constitutively active mutant (Rab7bQ67L), and we verified that myosin II was co-immunoprecipitated by Rab7b (Fig. 1B). Notably, Rab7bQ67L co-immunoprecipitated substantially more myosin II, compared with Rab7bwt, indicating the importance of the Rab GTP-bound form for the interaction.

We also investigated whether the interaction was specific for Rab7b, testing the ability of different purified Rab proteins to pull down myosin II from cell extracts. Therefore, His-tagged Rab7b, His-tagged Rab7a and His-tagged Rab9 were expressed in bacteria, then purified and incubated with total extracts of HeLa cells. As shown in Fig. 1C, only His-tagged Rab7b pulled down myosin II from total cell extracts, thus showing that the interaction is specific for Rab7b.

Subsequently, we investigated whether this interaction was direct. Purified bacterially expressed glutathione S-transferase (GST)-tagged myosin II tail was incubated together with His-tagged Rab7bQ67L, and then GST-tagged myosin II tail was precipitated using glutathione resin. Western blot analysis of the precipitated proteins revealed that His–Rab7b was able to specifically bind to GST–myosin-II, and no binding of His–Rab7b to GST protein alone was detected (Fig. 1D).

Altogether, our results demonstrate that Rab7b interacts directly with myosin II.

Rab7b transport is dependent on myosin II

As myosin motors are known to interact and regulate the transport of several Rab proteins (Seabra and Coudrier, 2004; Miserey-Lenkei et al., 2010; Roland et al., 2011; Lindsay et al., 2013), we next investigated whether the physiological relevance of the Rab7b–myosin-II interaction was linked to the regulation of

Journal of Cell Science (2014) 127, 4927–4939 doi:10.1242/jcs.155861

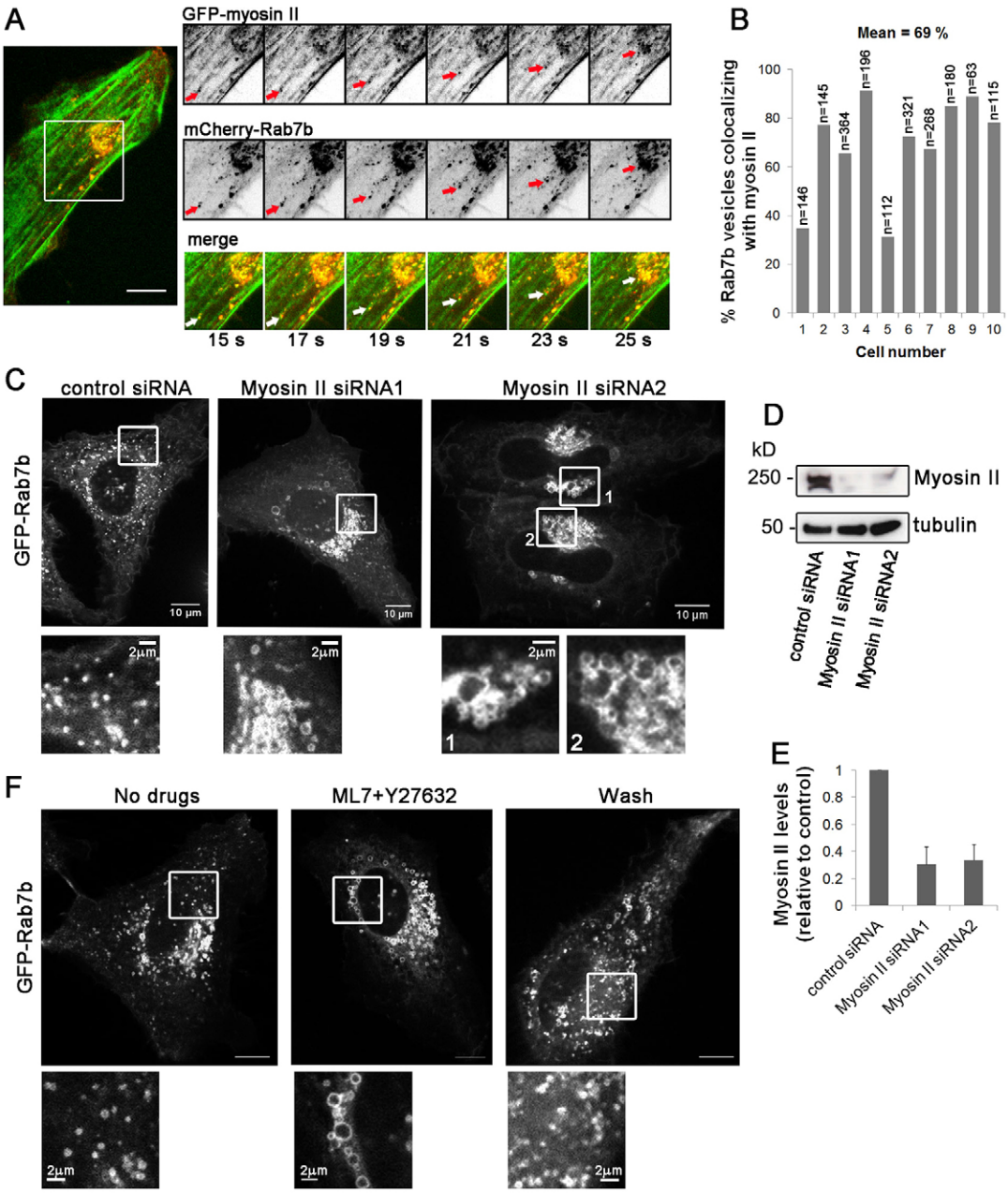

Fig. 2. Myosin II regulates the transport of Rab7b-positive endosomes. (A) HeLa cells co-transfected with GFP–myosin-II and mCherry–Rab7b were imaged by using a spinning-disk confocal microscope for the indicated time points. The red and white arrows indicate a vesicle positive for both GFP–myosin-II and mCherry–Rab7b moving toward the Golgi. See also supplementary material Movie 1. (B) Quantification of the overlap between Rab7b and myosin II. HeLa cells were transfected with GFP–myosin-II and mCherry–Rab7b. The percentage of Rab7b vesicles positive for myosin II was calculated by using an object-based colocalization analysis with ImageJ software. Total number of objects counted (n) is shown for ten different cells. (C) HeLa cells that had been treated with either control siRNA or two different siRNAs against myosin II (siRNA 1 and siRNA 2), and transfected with GFP–Rab7b, were imaged with a spinning-disk confocal microscope. Magnifications of the boxed areas are shown in the respective lower insets. See also supplementary material Movie 2. (D) HeLa cells treated with either control siRNA or two different siRNAs against myosin II were subjected to western blot analysis with antibodies against myosin II and tubulin as a loading control. (E) Quantification of myosin II expression. The intensities of the bands were quantified by using densitometry, normalized against the amount of tubulin, and plotted relative to the intensities obtained in cells transfected with control siRNA. The values represent the mean±s.d. of five independent experiments. (F) HeLa cells transfected with GFP–Rab7b were imaged using a spinning-disk confocal microscope before addition of the inhibitory mix ML7 with Y27632 (no drugs), 40 minutes after addition of 30 µM ML7 and 10 µM Y27632, and after washing away the inhibitory drugs (wash). Magnifications of the boxed areas are shown in the respective lower insets. Scale bars: 10 µm (A,F). See also supplementary material Movies 3–5.

intracellular trafficking. First, we studied the dynamics of green fluorescent protein (GFP)–myosin-II together with mCherry–Rab7b in live cells. Even though GFP–myosin-II was mostly associated with actin filaments, as expected, a small fraction was also visible in the proximity of the Golgi (Ikonen et al., 1997) (Fig. 2A; supplementary material Movie 1). Interestingly, time-lapse imaging revealed small Rab7b vesicles that were positive for myosin II moving toward the Golgi region, suggesting that the

Journal of Cell Science (2014) 127, 4927–4939 doi:10.1242/jcs.155861

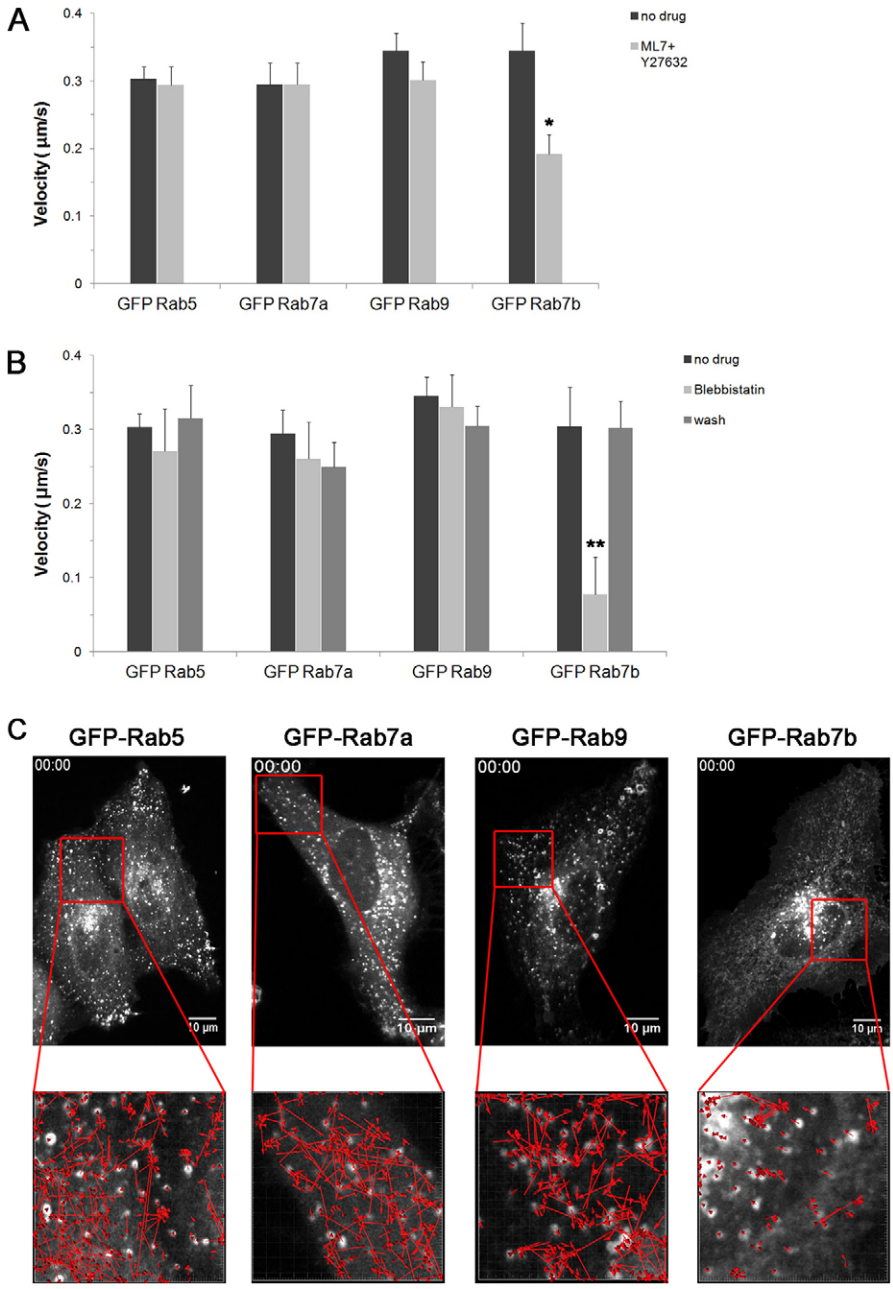

Fig. 3. Inhibition of myosin II specifically slows down Rab7b endosomes. (A–C) HeLa cells were transfected with GFP–Rab5, GFP–Rab7a, GFP–Rab9 or GFP–Rab7b, imaged by using a spinning-disk confocal microscope, and the velocity of single endosomes was quantified using the manual tracking plugin of the program ImageJ. The graphs represent the quantification of the mean velocity of single endosomes (A) both before addition (no drug) and after addition of the inhibitory mix ML7 and Y27632, and (B) before addition (no drug), after addition of blebbistatin, and after wash. At each of these conditions, a minimum of 30 endosomes (from three independent experiments) were measured over time. Error bars indicate mean±s.e.m. *$P<0.05$; **$P<0.01$. (C) HeLa cells were transfected with GFP–Rab5, GFP–Rab7a, GFP–Rab9 or GFP–Rab7b, and treated with blebbistatin (25 µM) for 40 minutes at 37°C before imaging with a spinning-disk confocal microscope. Imaging time (min:s) is indicated in the top left corner. In the lower insets, magnifications of the respective boxed areas are shown. Red arrows indicate endosomal movement tracked with IMARIS software over 3 minutes. Scale bars: 10 µM. See also supplementary material Movies 6, 7.

functional role of the interaction between Rab7b and myosin II is to mediate Rab7b transport along the cytoskeleton (Fig. 2A; supplementary material Movie 1). Quantification of more than 100 Rab7b-positive vesicles in cells transfected with mCherry–Rab7b and GFP–myosin-II showed that 69% of the Rab7b vesicles colocalize with myosin II (Fig. 2B).

To test for a potential role of myosin II in Rab7b-mediated transport, we followed, by using time-lapse video-microscopy, the dynamics of GFP–Rab7b in HeLa cells depleted for myosin II (Fig. 2C–E, supplementary material Movie 2). In cells knocked down for myosin II, GFP–Rab7b-positive endosomes were strongly clustered in the perinuclear region and significantly increased in size, compared to cells transfected with a control siRNA (Fig. 2C; supplementary material Movie 2). These enlarged structures were late endosomes, because they were positive for the late endosomal marker Lamp-1 (supplementary material Fig. S1). A similar effect was also observed, although to a lesser extent, by knocking down Rab7b expression (supplementary material Fig. S1). Interestingly, Rab7b-positive endosomes were also less mobile when cells were silenced using two different siRNAs that targeted different regions of myosin II (Fig. 2C–E; supplementary material Movie 2).

These results indicate the importance of myosin II for the proper intracellular distribution and dynamics of Rab7b-positive endosomes.

To further confirm the importance of myosin II in Rab7b-mediated transport, we used two different myosin II inhibitors that function with diverse mechanisms: (1) a mix containing ML7 (a myosin light chain kinase inhibitor) and Y27632 (Rho kinase inhibitor) or (2) blebbistatin (myosin II motor activity inhibitor). In the presence of the first, we observed a remarkable increase in the size of Rab7b-positive endosomes, and concomitantly, a

Journal of Cell Science (2014) 127, 4927–4939 doi:10.1242/jcs.155861

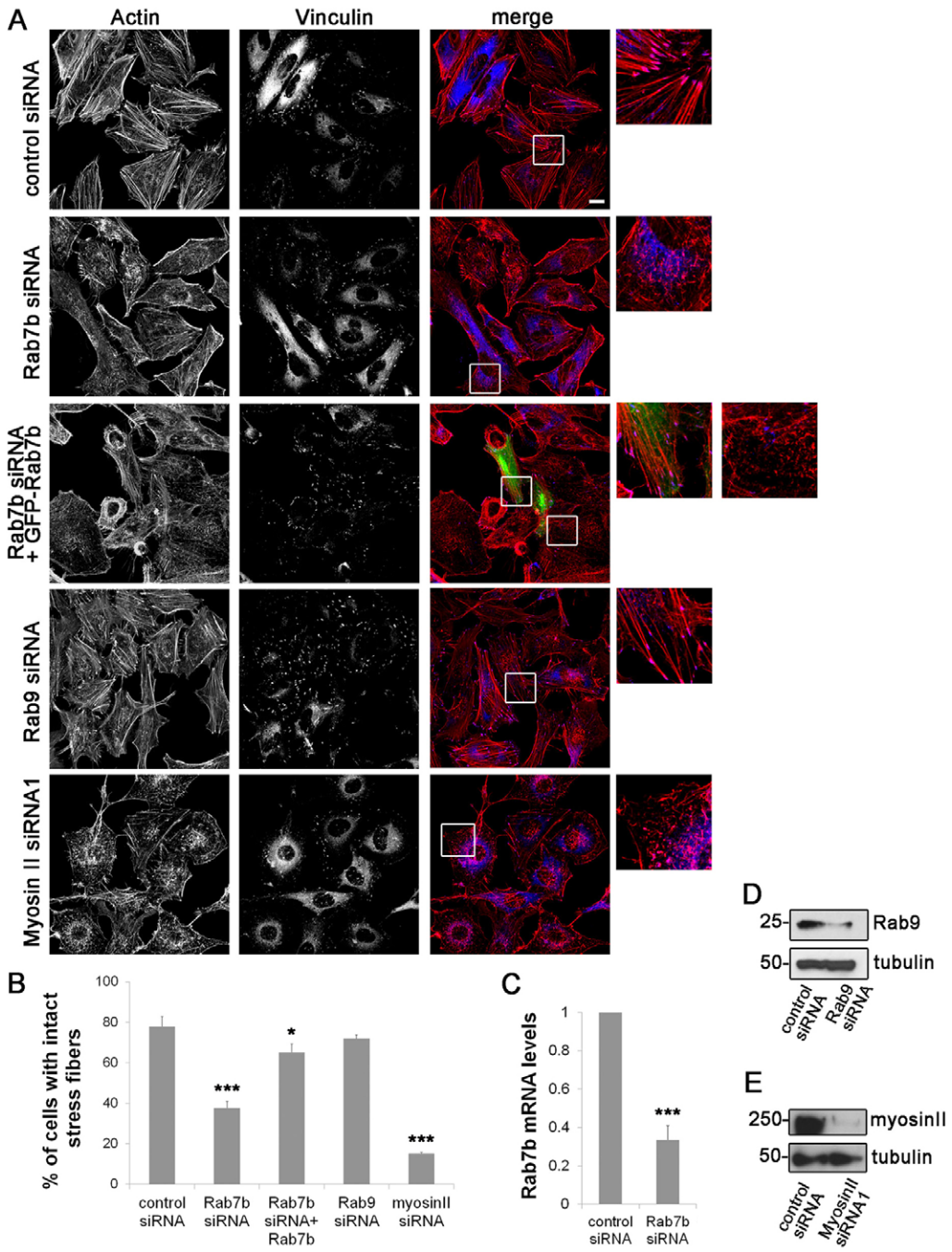

Fig. 4. Rab7b regulates stress fibers formation. (A) HeLa cells that had been transfected with control siRNA, siRNA against Rab7b, Rab9, myosin II, or depleted for Rab7b and transfected afterward with GFP–Rab7b were fixed and stained as indicated. The images represent maximum-intensity projections of *z*-stacks. Magnifications of the boxed areas are shown in the insets. Scale bar: 10 μm. (B) Quantification of the percentage of cells with intact stress fibers. Data represents the mean±s.e.m. of three independent experiments ($n>100$). *$P<0.05$; ***$P<0.001$. (C) Quantification of *Rab7b* transcript levels after silencing. Rab7b mRNA levels were quantified by using real-time RT-PCR in HeLa cells that had been transfected with control siRNA or siRNA targeted toward Rab7b. The level of *Rab7b* mRNA was normalized to the amount of actin and plotted relative to the levels of *Rab7b* mRNA in the control sample. Data represents the average of ten independent experiments ±s.d. ***$P<0.001$. (D) HeLa cells that had been treated with either control siRNA or siRNA against Rab9 were subjected to western blot analysis with antibodies against Rab9 and tubulin as a loading control. (E) HeLa cells treated with either control siRNA or siRNA against myosin II (Myosin II siRNA 1) were subjected to western blot analysis with antibodies against myosin II and tubulin as a loading control.

clustering in the perinuclear region, as in cells that had been depleted of myosin II (Fig. 2F). Moreover, we observed a specific and marked reduction in the velocity of Rab7b endosomes (0.19 μm/s) of almost 50% compared with that of the untreated cells (0.34 μm/s) (Fig. 3A; supplementary material Movie 5). These effects were specific for Rab7b, as the inhibitors did not affect Rab5, Rab7a or Rab9 (supplementary material Fig. S2, Fig. S3A; Movies 3, 4).

In cells that had been treated with the second inhibitor, blebbistatin, this reduction in velocity was even stronger, with a

Journal of Cell Science (2014) 127, 4927–4939 doi:10.1242/jcs.155861

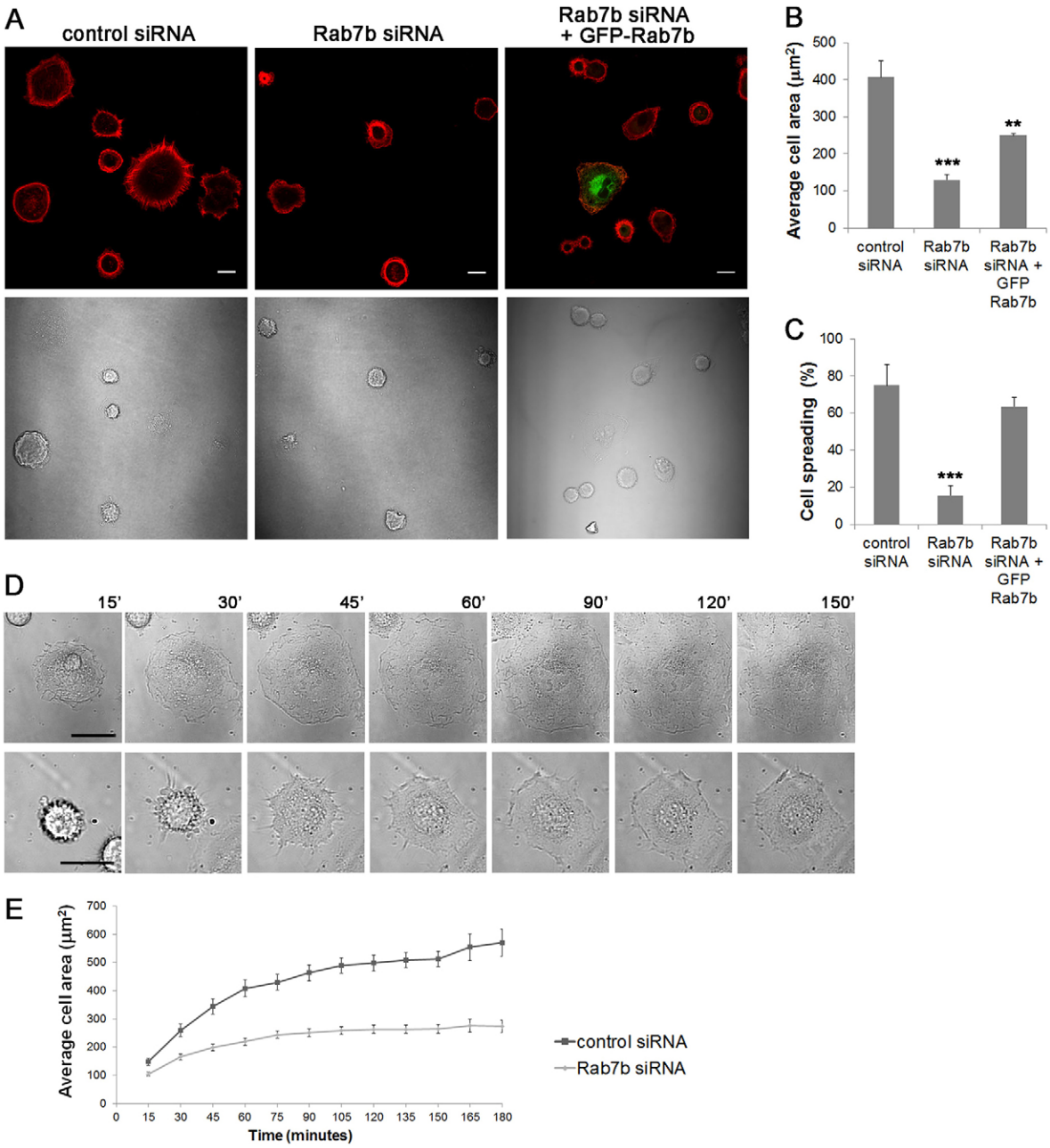

Fig. 5. Depletion of Rab7b suppresses cell spreading. (A) HeLa cells transfected with control siRNA, siRNA against Rab7b, or depleted for Rab7b and transfected afterward with GFP–Rab7b were plated onto fibronectin-coated coverslips and left to adhere for 1 hour. Samples were subsequently fixed and stained with Rhodamine-conjugated phalloidin and imaged by using fluorescence microscopy (upper panel). Lower panel shows transmission images for comparison. Scale bars: 10 μm. (B) Quantification of the average cell area (in μm^2) of HeLa cells transfected with control siRNA, siRNA against Rab7b, or depleted for Rab7b and transfected afterward with GFP–Rab7b after 1 hour of adhesion onto fibronectin. Data represents the mean±s.d. of three independent experiments ($n>100$). $^{**}P<0.01$; $^{***}P<0.001$. (C) The graph shows the percentage of fully spread cells (area >200 μm^2) 1 hour after plating onto fibronectin-coated coverslips. Data represents the mean±s.d. of three independent experiments ($n\geq100$). $^{***}P<0.001$. (D) Control cells (upper panels) and Rab7b-depleted cells (lower panels) were plated onto fibronectin-coated dishes, and cell spreading was imaged every 15 minutes (total time after plating is shown above the image). Scale bars: 10 μm. See also supplementary material Movie 8. (E) Quantification of the average cell area (in μm^2) of HeLa cells transfected with control siRNA or siRNA against Rab7b during adhesion onto fibronectin-coated dishes at the indicated time points. Data represents the mean±s.e.m. of three independent experiments ($n>100$).

specific decrease of velocity for Rab7b-positive endosomes to 0.08 μm/s, almost fourfold less than the control (Fig. 3B,C; supplementary material Movie 7). This effect was reversible, as washing away the inhibitor restored the initial endosomal speed. The effect was also specific for Rab7b, as Rab5, Rab7a and Rab9 were unaffected (Fig. 3B,C; supplementary material Movie 6). The reduction in the velocity of Rab7b endosomes is consistent with an active role for myosin II as a molecular motor that mediates Rab7b movement along the actin cytoskeleton.

In the presence of blebbistatin, we again observed clustering of Rab7b endosomes in the perinuclear region, but no significant differences in the endosomal size. This difference in the effect of the two inhibitors on endosomal size might, however, be explained by the different mechanisms of action of the drugs

Journal of Cell Science (2014) 127, 4927–4939 doi:10.1242/jcs.155861

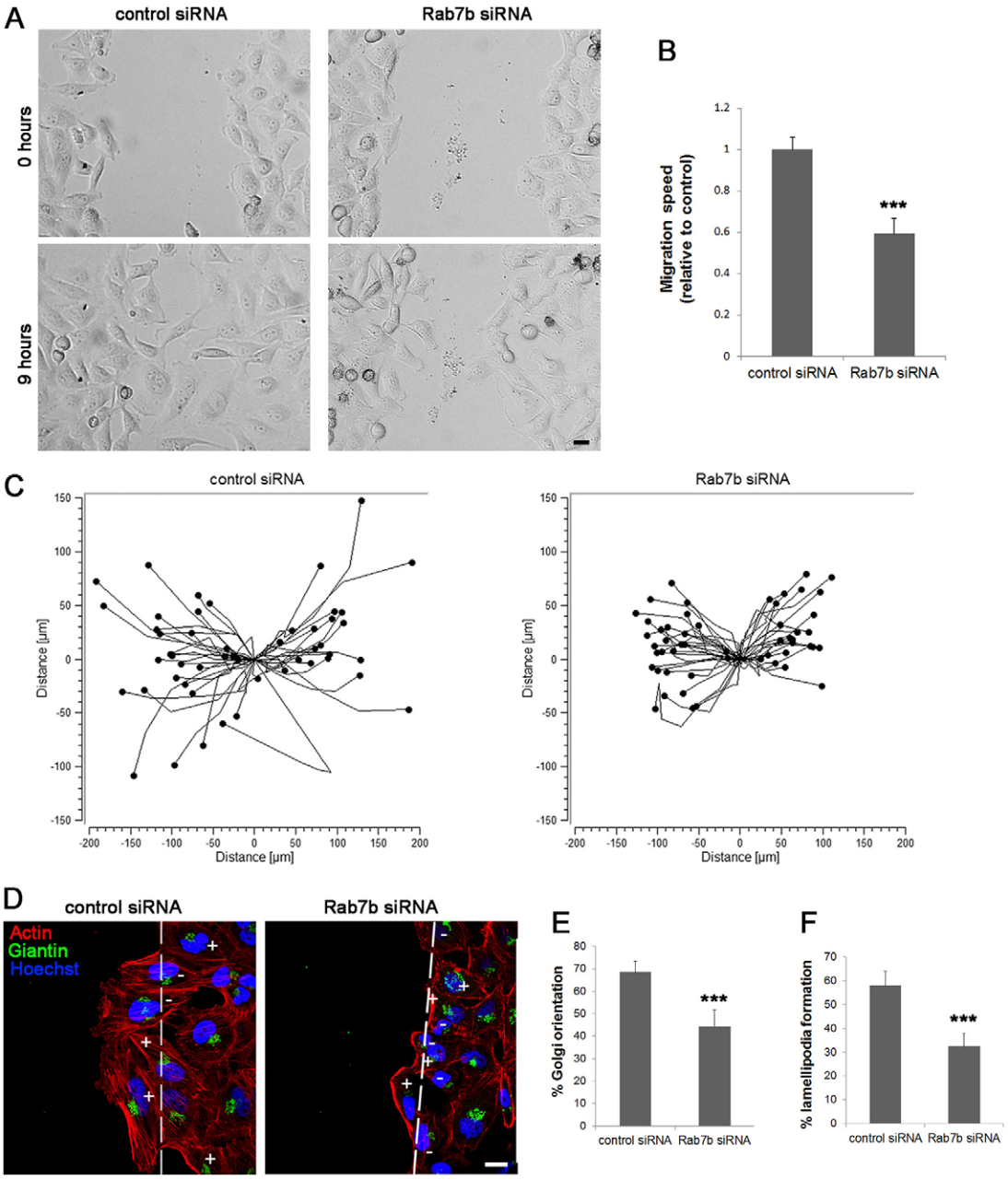

Fig. 6. Rab7b silencing delays cell migration and polarization in response to wound. (A) Wound healing assay of HeLa cells that had been transfected with control siRNA or siRNA against Rab7b at time 0 (0 hours) and after 9 hours. (B) Quantification of the migration speed of control cells and Rab7b-depleted cells in wound healing assays. Data represents the mean±s.d. of three independent experiments ($n \geq 100$). (C) Representative track plots of the distances of migration of control cells (left plot) or Rab7b-depleted cells (right plot) in a wound healing assay. The movement of single cells into the wound was followed using manual tracking software. Individual tracks are shown so that each starts at the origin (distance 0). (D) Confluent monolayers of HeLa cells that had been transfected with control siRNA or siRNA against Rab7b were scratched with a pipette tip and fixed 2 hours later. Cells were immunostained with an antibody against giantin; actin was labeled with Rhodamine-conjugated phalloidin and nuclei with Hoechst 33258. White lines indicate the wound. The Golgi is labeled as + if the majority of it lies within a 120° angle facing the wound or as − if not. (E) Quantification of the percentage of cells with Golgi located in the 120° angle facing the wound. The graph shows the mean±s.d. of four independent experiments ($n \geq 100$). (F) Quantification of the percentage of the cells emanating lamellipodia into the wound area. The graph shows the mean±s.d. of four independent experiments ($n \geq 100$). ***$P<0.001$. Scale bars: 20 µm (A); 10 µm (D).

because ML7 and Y27632, but not blebbistatin, interfere with phosphorylation of myosin II (Wang et al., 2008; Shutova et al., 2012).

To gain more insights into the mechanisms that cause these altered Rab7b phenotypes in the absence of functional myosin II, we examined the actin cytoskeleton in the presence of these drugs. After treatment with blebbistatin, a fraction of stress fibers was still visible, whereas the mix of ML7 and Y27632 completely destroyed actin filaments (Katoh et al., 2001a) (supplementary material Fig. S3). Notably, in the presence of this mix of inhibitors, we observed actin puncta on Rab7b endosomes (supplementary material Fig. S3). As actin puncta on

Journal of Cell Science (2014) 127, 4927–4939 doi:10.1242/jcs.155861

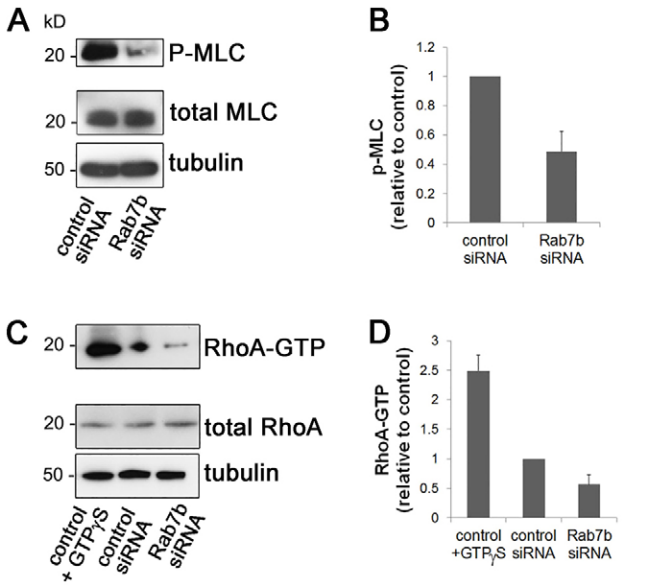

Fig. 7. Rab7b regulates MLC phosphorylation by interfering with RhoA activity. (A) Lysates from HeLa cells that had been transfected with either control siRNA or siRNA against Rab7b were subjected to western blot analysis using antibodies against phosphorylated myosin light chain (P-MLC), total MLC and tubulin (as a loading control). (B) Quantification of P-MLC levels in control and Rab7b-depleted cells. The intensities of the bands from the western blot were normalized to the amount of tubulin and plotted relative to the intensities of P-MLC in the control siRNA sample. Quantification is based on three independent experiments and were determined by using ImageQuant Software (Amersham). Error bars represent the mean±s.e.m. (C) Lysates from HeLa cells that had been transfected with either control siRNA or siRNA against Rab7b were mixed with GST–Rhotekin-RBD bound to glutathione-agarose beads to precipitate the active form (GTP-bound) of RhoA. As a positive control, cells were loaded with GTPγS. The immunoprecipitate samples were subjected to western blot analysis using antibodies against RhoA and tubulin (loading control). (D) Quantification of the levels of active RhoA in control and Rab7b-depleted cells. Intensities of the bands from the western blot were quantified with ImageQuant, normalized to the amount of tubulin and plotted relative to the intensities of GTP-bound RhoA in the control sample. The values represent the mean±s.e.m. of five independent experiments.

endosomes are important for carrier formation (Morel et al., 2009), this suggests that the enlarged size of Rab7b endosomes is caused by a defect in fission due to the lack of actomyosin force to efficiently drive membrane scission.

Taken together, all these observations show that myosin II is required for the correct dynamics of Rab7b-positive endosomes.

Rab7b regulates stress fiber organization

As myosin is an actin motor, we depleted HeLa cells for Rab7b by using siRNA, and we analyzed the actin cytoskeleton using confocal microscopy (Fig. 4). Strikingly, in Rab7b-depleted cells, we observed a significant reduction in the number of stress fibers, together with a simultaneous increase in the number of actin foci. Indeed, only in 38% of the cells silenced for Rab7b was it possible to detect intact actin fibers, whereas they were present in 78% of the control cells (Fig. 4B). The specificity of the effect was further supported by the finding that stress fibers recovered in cells that had been first silenced for Rab7b and then transfected with GFP–Rab7b, and the percentage of cells with normal actin fibers went up to 65% (Fig. 4A,B).

As expected, we also observed stress fiber disruption after silencing myosin II (Fig. 4A,E). Furthermore, by knocking down Rab9, which also regulates the late endosome to TGN transport, we were still able to detect intact stress fibers in more than 70% of the cells (Fig. 4), indicating that the disruption of stress fibers is a specific consequence of Rab7b depletion.

These results suggest that Rab7b controls actin cytoskeleton organization through an association with myosin II.

Loss of Rab7b reduces cell spreading and delays wound closure

Having observed that Rab7b interferes with actin organization, we next investigated whether, by regulating actomyosin organization, Rab7b influences processes that require actin cytoskeleton rearrangements, such as cell adhesion and migration.

We therefore measured the ability of the cells to spread out onto fibronectin-coated dishes. The average area of control cells 1 hour after plating was 407 μm^2 (and 75% of the cells had an area $>200\ \mu m^2$), whereas Rab7b-depleted cells showed impairment in their ability to spread. Indeed, only 15% had an area $>200\ \mu m^2$, with an average area of 129 μm^2, meaning 3.4-fold less than that of control cells (Fig. 5A–C).

To validate that the inability of cells knocked down for Rab7b to spread onto fibronectin was due to a specific role of Rab7b, we performed a rescue experiment. The transient expression of GFP–Rab7b in Rab7b-knockdown cells was sufficient to re-induce cell spreading onto fibronectin (63.5% of cells had an area $>200\ \mu m^2$, with a total average area of 249 μm^2), confirming the involvement of Rab7b in cell adhesion (Fig. 5A–C).

F-actin staining revealed that cells knocked down for Rab7b had reduced membrane protrusions at the cell periphery in response to adhesion onto fibronectin (Fig. 5A). To check whether this effect was the consequence of a slower spreading rate (cells at an earlier stage of spreading are characterized by fewer membrane protrusions), we next used live imaging to follow cell adhesion and spreading (Fig. 5D,E; supplementary material Movie 8). Interestingly, cells that had been depleted for Rab7b showed not only less membrane ruffling, even at later time points, but also constantly reduced spreading compared with that of control cells (Fig. 5D,E; supplementary material Movie 8), indicating that Rab7b is necessary for correct cell spreading.

As cell adhesion is an important step in the process of cell migration, we performed a wound-healing assay to investigate whether Rab7b depletion also affects cell motility. A confluent monolayer of HeLa cells transfected with a control siRNA or an siRNA against Rab7b was scratched, and the migration of the cells toward the wound area was imaged and quantified. Interestingly, Rab7b-depleted cells were slower compared with control cells, showing a 40% reduction in the average single-cell speed (Fig. 6A–C; supplementary material Movie 9).

We confirmed that the delayed cell migration was a consequence of Rab7b depletion on actin cytoskeleton dynamics, because we could observe, in parallel, a significant decrease of filamentous actin structures (lamellipodia) at the leading edge after staining migrating cells for F-actin. Indeed, although almost 60% of control cells extended broad lamellipodia at the leading edge 2 hours after the wound, only 32% of the Rab7b-depleted cells showed membrane protrusions into the open wound area (Fig. 6D,E).

To further test whether Rab7b knockdown also interferes with cell polarization, we measured the cell polarity during migration,

Journal of Cell Science (2014) 127, 4927–4939 doi:10.1242/jcs.155861

based on the orientation of the Golgi into the direction of the wound. When cells polarize for migration, the Golgi reorientates from a random perinuclear position to the third of the cell area that occupies the space between the nucleus and the wound-edge area (Kupfer et al., 1982; Bisel et al., 2008). The Golgi reorientation was strongly affected in Rab7b-depleted cells, where only 44% of the cells showed an orientation toward the wound-edge area, compared with control cells, where 68% of the cells responded positively to Golgi reorientation (Fig. 6D,E). This, along with the results of decreased cell migration in Rab7b-depleted cells, indicates that Rab7b plays a role in cell polarization in response to a wound.

All together, these data show that, by acting on actin cytoskeleton, Rab7b is important for the establishment of cell polarity in order to induce cell adhesion and migration.

Rab7b regulates actin organization by controlling myosin phosphorylation

Stress fiber formation, cell adhesion, polarization and migration are all processes where the reorganization of the actin cytoskeleton and actomyosin contractility is required (Naumanen et al., 2008; Parsons et al., 2010; Rottner and Stradal, 2011). As we have demonstrated that these cellular functions are all affected by Rab7b depletion and that they are dependent on MLC phosphorylation (Watanabe et al., 2007; Hirata et al., 2009), we next investigated whether Rab7b knockdown altered MLC phosphorylation status. Residue Ser19 is the primary phosphorylation site of MLC, and phosphorylation of MLC at Ser19 increases both the actin-activated Mg-ATPase activity and the stability of myosin II filaments (Amano et al., 1996; Bresnick, 1999). Using an antibody that specifically recognizes phosphorylated MLC on residue Ser19, we found that MLC phosphorylation was strongly downregulated in Rab7b-depleted cells, whereas the levels of total MLC remained unchanged (Fig. 7A,B). As expected, we observed the same effect after myosin II depletion, using siRNAs targeting the myosin heavy chain (supplementary material Fig. S4A,B).

MLC phosphorylation is regulated by several kinases, with ROCK (Rho kinase) as one of the most important (Amano et al., 1996; Katoh et al., 2001b). ROCK is a direct target of RhoA, a small GTPase that works as a molecular switch cycling between an inactive GDP-bound and an active GTP-bound form (Matsui et al., 1996). In its active state, RhoA stimulates the formation of stress fibers and cell migration through effectors, such as ROCK (Amano et al., 1997; Riento and Ridley, 2003; Worthylake and Burridge, 2003). The Rho GTPase and its downstream targets are therefore responsible, through phosphorylation of MLC, for controlling these cytoskeleton dynamics.

To determine whether Rab7b influences MLC phosphorylation by acting on the RhoA–ROCK pathway, we measured RhoA activity by using a pulldown assay. Lysates from control cells or Rab7b-depleted cells were incubated with the GST-tagged Rho-binding domain (RBD) of Rhotekin bound to glutathione agarose beads, and affinity-precipitated proteins were probed for RhoA-GTP by using immunoblot analysis. As shown in Fig. 7C,D, the activity of RhoA was strongly decreased (more than 60%) in Rab7b-depleted cells. Depletion of myosin II, instead, decreased RhoA activity with a maximum of 30% (supplementary material Fig. S4C,D).

In conclusion, our results reveal that, by interfering with RhoA activation, Rab7b can control the phosphorylation of MLC and thereby actin cytoskeleton organization (Fig. 8).

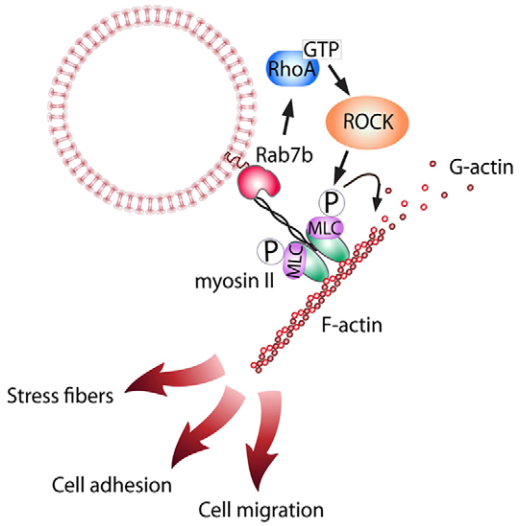

Fig. 8. Model of Rab7b–myosin-II regulation of actin remodeling. Rab7b regulates MLC phosphorylation by modulating RhoA activity, and therefore actin remodeling, including the formation of stress fibers and the actin cytoskeleton reorganization that is necessary for processes such as cell adhesion and migration.

DISCUSSION

We have recently demonstrated that the small GTPase Rab7b regulates endosome-to-TGN transport (Progida et al., 2010; Progida et al., 2012). Depletion of Rab7b, or the expression of the dominant-negative or constitutively active mutants, disturbs this transport pathway (Progida et al., 2010; Progida et al., 2012). However, little is known about the function of this Rab or its interaction partners.

In a screen to identify Rab7b interacting proteins, we discovered myosin II as a direct effector. Rab proteins, in their active state, bind effectors, and several Rab proteins are known to bind cytoskeletal motors that ensure their directional transport (Seabra and Coudrier, 2004; Horgan and McCaffrey, 2011). In agreement with this, here we provide evidence that myosin II behaves as an effector that regulates Rab7b dynamics. Indeed, we show that, by interfering with this molecular motor through either siRNA transfection or chemical inhibitors, myosin II is important for both the fission of Rab7b-positive endosomes (as its inhibition causes enlargement of Rab7b endosomes) and movement (visualized through a block of endosome motility).

In particular, after destroying actin stress fibers through inhibition of MLC phosphorylation, we observed enlarged endosomes with actin puncta on the membrane (supplementary material Fig. S3). This suggests that myosin II anchors Rab7b-positive membranes onto the actin cytoskeleton and that the phosphorylation inhibition prevents the actin polymerization that is necessary to generate the force needed to drive membrane fission.

It is known that actomyosin filament contraction is involved in carrier scission and that the presence of actin patches on endosomal membranes is important for driving the biogenesis of transport intermediates (Morel et al., 2009; Anitei and Hoflack, 2012). Thus, our data indicate that the interaction between Rab7b and myosin II is important for both the fission and the transport of Rab7b endosomes.

The Rab family of proteins belongs to the Ras superfamily of small GTPases. This superfamily comprises five main families,

Journal of Cell Science (2014) 127, 4927–4939 doi:10.1242/jcs.155861

each of them characterized by a different function despite a conserved structure and similar biochemical properties (Goitre et al., 2014). Among them, the Rho family members are key regulators of the actin cytoskeleton and cell migration, whereas the Arf and Rab families are important regulators of the intracellular transport (Stenmark, 2009; Donaldson and Jackson, 2011; Hall, 2012). Interestingly, an additional function for the Arf family has been identified recently. Indeed, members of this family are also regulators of actin remodeling and cell migration (Myers and Casanova, 2008; Lewis-Saravalli et al., 2013).

Here, we have shown that, similar to Arfs, a member of the Rab family of small GTPases, Rab7b, by interacting with myosin II, is able to control not only intracellular trafficking but also actin cytoskeleton dynamics. Specifically, silencing of Rab7b by using RNAi reduces stress fiber formation, cell adhesion and cell migration. In addition, formation of lamellipodia at the leading edge is attenuated in migrating Rab7b-depleted cells.

In line with the requirement of actin contractility for the Golgi positioning during cell migration (Gomes et al., 2005), a decrease in the reorientation of the Golgi toward the wound was observed in cells in which Rab7b had been knocked down (Fig. 6D,E). However, as Rab7b and myosin II are involved in a plethora of cellular functions, we cannot exclude that the effects on cell spreading and migration could also be the outcome of a more complex signaling network.

As the processes dependent on actomyosin contractility are regulated by MLC phosphorylation, we investigated whether Rab7b, by interacting with myosin II, influences this phosphorylation. Importantly, the levels of phosphorylated MLC were strongly downregulated in Rab7b-depleted cells (Fig. 7A,B), indicating that the mechanism used by Rab7b to regulate actin cytoskeleton remodeling is through the control of MLC phosphorylation.

ROCK is one of the main kinases that regulate MLC phosphorylation, and its inhibition results in phenotypes similar to those observed upon Rab7b depletion, such as disrupted stress fibers and reduced cell adhesion (Amano et al., 1997; Katoh et al., 2001b). ROCK is activated by another member of the Ras superfamily of small GTPases, RhoA. To activate the kinase, RhoA has to be in an active GTP-bound state (Matsui et al., 1996). Strikingly, the fraction of GTP-bound RhoA was strongly reduced upon Rab7b depletion (Fig. 7C,D). This suggests that Rab7b regulates RhoA and explains the decrease in MLC phosphorylation in Rab7b-depleted cells. In summary, our results support a role for Rab7b in the regulation of actin cytoskeleton organization by mediating MLC phosphorylation through RhoA activation (Fig. 8).

In line with our data, a very recent report suggests that Rab7b might associate with the calpain and myosin pathway in platelets, small cytoplasmic fragments where the actin cytoskeleton remodeling is crucial (Tsai et al., 2014). We now unequivocally demonstrate that Rab7b directly interacts with myosin II, and we characterize the functional role of this interaction in both intracellular trafficking and actin cytoskeleton organization. We show that Rab7b triggers myosin II activation by stimulating phosphorylation of residue Ser19 of MLC, through the activation of RhoA, revealing that a Rab protein modulates the activity of another family of small GTP-binding proteins, the Rho family. Interestingly, other small GTPases, Arf1 and Arf6, known to regulate endosomal transport (Kobayashi and Fukuda, 2013; Nakai et al., 2013; Hongu and Kanaho, 2014), also control cytoskeletal organization through crosstalk with Rho-family GTPases (Lewis-Saravalli et al., 2013; Schlienger et al., 2014). Although the exact mechanism of Rho activation remains to be elucidated, it could occur in several ways, such as through the recruitment of Guanine nucleotide exchange factors (GEFs) or the downregulation of Rho GTPase-activating proteins (GAPs).

Other Rab proteins that interact with members of the myosin family also interfere with the process of cell migration (Seabra and Coudrier, 2004; Allaire et al., 2013). However, their effects on cell migration have so far been investigated only in connection to the well-established role of Rabs in intracellular trafficking (Kawauchi et al., 2010; Mai et al., 2011; Linford et al., 2012; Allaire et al., 2013; Wiesner et al., 2013).

By illuminating the role of a Rab protein in controlling actin remodeling, our results also open new possibilities for those Rab proteins that have been found to have a role in cell migration.

In conclusion, by demonstrating that Rab7b interacts directly with myosin II to regulate actin organization and endosome dynamics, we propose the novel mechanism by which a Rab protein controls both intracellular trafficking and cytoskeleton remodeling, revealing an unexpected role for this protein family.

MATERIALS AND METHODS

Cell culture

HeLa cells were grown in Dulbecco's modified Eagle's medium (DMEM) supplemented with 10% fetal calf serum (FCS), 2 mM L-glutamine, 100 U/ml penicillin and 100 µg/ml streptomycin.

Mononuclear cells were isolated from buffy-coats from healthy blood donors through density gradient centrifugation by using Lymphoprep (Axis Shield). Blood components (buffy-coats) from anonymous blood donors were obtained from the local blood bank (Section for Immunology and Blood Transfusion, Ullevål University Hospital, Oslo, Norway) according to the guidelines of the local blood bank approved by the Norwegian Regional Committee for Medical Research Ethics. MDDCs were generated from plastic adherent or directly isolated monocytes (Monocyte Isolation Kit II, Miltenyi Biotec) through culture for 6 days in RPMI media containing 100 ng/ml granulocyte-macrophage colony-stimulating factor (GM-CSF; Immunotools) and 20 ng/ml IL-4 (Invitrogen, Life Technologies) supplemented with 10% FCS, 2 mM L-glutamine, 100 U/ml penicillin and 100 µg/ml streptomycin. GM-CSF and IL-4 were replenished every 2–3 days.

Constructs, antibodies and inhibitors

pEGFP-Rab7bwt, pcDNA-2XHA-Rab7bwt, pcDNA-2XHA-HA-Rab7bQ67L, pcDNA-mCherry-Rab7b, pET16b His-Rab7a, pET16b His-Rab7b, pET16b His-Rab7bQ67L and pET16b His-Rab9 have been described previously (Spinosa et al., 2008; Progida et al., 2010; Progida et al., 2012). pEGFP-myosin II A was obtained from Robert Adelstein through Addgene (plasmid no. 11347) (Wei and Adelstein, 2000). pEGFP-Rab5 and pEGFP-Rab7a were a gift from Cecilia Bucci (Bucci et al., 2000). pEGFP Rab9 was constructed by amplifying Rab9 by PCR using the following primers containing, respectively, a *Bgl*I and a *Pst*I restriction site: Rab9-for 5′-AGAGAAGATCTATGGCAGGAAAATCTTCAC-TTT-3′ and Rab9-rev 5′-AGAGACTGCAGTCAACAGCAAGATGAG-CTAGGCT-3′. The fragment was then inserted into pEGFP-C1 that had been cut with *Bgl*I and *Pst*I. For the construction of pGBKT7 Rab7bΔC, where the two C-terminal cysteine residues were deleted to avoid post-translational prenylation, the coding sequence of Rab7b was amplified by using PCR with the following primers containing, respectively, an *Eco*RI and a *Sal*I restriction site: Rab7b-for 5′-AGAGAGAATT-CATGAATCCCCGGAAGAAGGT-3′ and Rab7b-rev 5′-AGAGAGA-CGTCGACTCTGCTCCTTGACTGGTCTG-3′. The Rab7bΔC fragment was then cloned into the pGBKT7 plasmid that had been cut with *Eco*RI and *Sal*I.

The myosin II A heavy chain tail (amino acids 1795–1960) was amplified by using PCR with the following oligonucleotides:

Journal of Cell Science (2014) 127, 4927–4939 doi:10.1242/jcs.155861

5′-AGAGAGGATCCCAGGAGATGGAGGGCACTGTC-3′ and 5′-TTC-TCTGAATTCTTATTCGGCAGGTTTGGCCTCA-3′, and then cloned in frame into the pGEX2T vector using *Bam*HI and *Eco*RI restriction sites to obtain a plasmid for the bacterial expression of the GST–myosin-II-tail. All the newly made constructs were sequence verified.

Primary antibodies used in this study were anti-HA (1:1500, catalog number ab9110), anti-giantin (1:1000, catalog number ab24586) and anti-non-muscle myosin IIA (1:3000, catalog number ab24762) from Abcam; anti-GST (1:1000, catalog number G1160), anti-MLC (1:40, catalog number M4401) and anti-vinculin (1:100, catalog number V9131) from Sigma-Aldrich; anti-myosin-light-chain phosphorylated at residue Ser19 (1:300, catalog number 3671, Cell Signaling Technology), anti-RhoA (1:500, catalog number ARH03, Cytoskeleton), anti-Rab7b (1:300, catalog number H00338382-M01, AbNova), anti-His (1:5000, catalogue number MCA1396, AbD Serotec) and anti-tubulin (1:10,000, catalog number 13-8000, Life Technologies). Mouse IgG2aK was purchased from BD Pharmingen (catalog number 555571). Secondary antibodies conjugated with Alexa-Fluor-488 or -647 (Life Technologies) were used at dilution 1:200 for immunofluorescence analyses. Secondary antibodies conjugated with horseradish peroxidase (GE Healthcare) were used at 1:5000 for immunoblotting.

ML7 and Y27632 were purchased from Calbiochem, and blebbistatin from Sigma-Aldrich. For the experiments, 30 µM ML7 and 10 µM Y27632, or 25 µM blebbistatin, was added to the cell medium for 40 minutes at 37℃ under 5% CO_2.

Transfection and RNAi

Cells were transiently transfected at 50–70% confluence using FuGENE 6 (ProMega) according to the protocol provided by the manufacturer. The cells were analyzed 24 hours post transfection.

Transfection of HeLa cells with siRNA was performed as described previously (Progida et al., 2007). Briefly, HeLa cells were plated 1 day before transfection in 6-cm dishes (~4×10^5 cells/dish). Cells were transfected with siRNA using Oligofectamine (Invitrogen) for 72 hours, replated, and left for another 48 hours before further experiments were performed.

For RNAi, we used the following oligonucleotides: Rab7b siRNA, sense sequence 5′-GUAGCUCAAGGCUGGUGUATT-3′ and antisense sequence 5′-UACACCAGCCUUGAGCUACTT-3′. For myosin II siRNA 1, sense sequence 5′-GAACAAGCAUGAGGCAAUGTT-3′ and antisense sequence 5′-CAUUGCCUCAUGCUUGUUCTT-3′. For myosin II siRNA 2, sense sequence 5′-CAAGGAGCUUAAGGUC-AAGTT-3′ and antisense sequence 5′-CUUGACCUUAAGCUCCUU-GTT-3′. For Rab9 siRNA, sense sequence 5′-GUUUGAUACCCAGC-UCUUCTT-3′ and antisense sequence 5′-GAAGAGCUGGGUAUCA-AACTT-3′.

As a negative control we used a scrambled sequence: control siRNA, sense sequence 5′-ACUUCGAGCGUGCAUGGCUTT-3′ and antisense sequence 5′-AGCCAUGCACGCUCGAAGUTT-3′.

All chemically synthesized oligonucleotides were purchased from a commercial supplier (Eurofins MWG Operon).

RNA procedures and quantitative real-time RT-PCR

Total RNA was extracted from HeLa cells by using the PerfectPure RNA Cell Kit (5Prime), according to the manufacturer's instructions.

cDNA was synthesized with use of the First Strand cDNA Synthesis Kit (Roche). Cytosolic RNA (1 µg) from cells and 60 µM random hexamer primers were mixed and heated at 65℃ for 10 minutes before immediate cooling on ice. First strand cDNA synthesis was then performed using 10 U reverse transcriptase, 20 U Ribonuclease inhibitor and 1 mM dNTPs for 10 minutes at 25℃, followed by 30 minutes at 55℃. The reactions were stopped by heat inactivation at 85℃ for 5 minutes.

Following each reverse transcription, cDNA was amplified and quantified by using real-time reverse transcriptase (RT)-PCR with the LightCycler 480 SYBR Green I master mix and the LightCycler 480 real-time PCR system (Roche). Primers for *Rab7b* (forward primer, 5′-GGCCAGCATCCTCTCCAAGATTATC-3′; reverse primer, 5′-GATG-CAGCCATCGGAGCCCTTGT-3′) and for human actin (forward primer, 5′-CTGACTGACTACCTCATGAAGATCCT-3′; reverse primer, 5′-CTTAATGTCACGCACGATTTCC-3′) were purchased from Eurofins MWG Operon.

The PCR program was as follows: 1 cycle 3 minutes at 94℃; 35 cycles 30 seconds at 94℃, 30 seconds at 60℃, and 30 seconds at 72℃; 1 cycle 6 seconds at 75℃. The specificity and the identity of the PCR product was checked by performing a melting-curve test. Actin transcript levels were used for the normalization of the samples.

Yeast two-hybrid screening

A yeast two-hybrid screen of a human cDNA library from heart using human Rab7bΔC cloned into pGBKT7 as a bait was performed by DFKZ (German Cancer Research Center).

Co-immunoprecipitation and western blot experiments

For immunoprecipitation, Dynabead protein G (Invitrogen) was used according to the manufacturer's instructions. Briefly, 0.6 µg of Dynabeads were washed with RIPA buffer and incubated with anti-Rab7b or IgG2aK (negative control) antibodies for 60 minutes at room temperature with end-over-end rotation. After washing, precleared cell lysates were added to the Dynabeads and incubated for 90 additional minutes with end-over-end rotation. Immunoprecipitated samples were loaded on SDS-PAGE gels and analyzed by western blotting.

For western blot experiments, proteins were separated using SDS-PAGE, blotted onto a Immobilion polyvinylidene fluoride (PVDF) membrane (Millipore) and probed with the specific primary antibodies diluted in 2% blotting grade non-fat dry milk (Bio-Rad) followed by horseradish peroxidase (HRP)-conjugated secondary antibodies (1:5,000; GE Healthcare). Proteins were visualized using the ECL system (GE Healthcare). Protein levels were quantified by using densitometry using ImageQuant TL software (GE Healthcare).

Protein purification, pulldown and direct interaction experiments

GST, GST–myosin-II and His-tagged Rab proteins were expressed in *Escherichia coli* BL21 (DE3) (Agilent Technologies) after induction with 0.5 mM IPTG for 4 hours at 22℃. Expressed His–Rab fusion proteins were purified from the bacterial soluble fraction using His-tagged isolation Dynabeads (Invitrogen) in the presence of 50 mM sodium phosphate, pH 8, 300 mM NaCl and 0.01% Tween-20, according to the manufacturer's protocol. To activate Rab GTPases, purified His-tagged Rabs bound to Dynabeads were loaded with 0.1 mM GTPγS.

Purification of GST and GST–myosin-II was performed according to the manufacturer's protocol (GE Healthcare).

For pulldown experiments, 20 µg of GTPγS-His–Rab fusion proteins bound to Dynabeads were incubated with precleared HeLa cell lysates for 30 minutes at 4℃ and then washed six times with buffer containing 3.25 mM sodium phosphate, pH 7.4, 70 mM NaCl and 0.01% Tween-20. Bound proteins were eluted with elution buffer (50 mM sodium phosphate, pH 8.0, 300 mM NaCl, 0.01% Tween-20, 300 mM imidazole). Samples were analyzed by using SDS-PAGE and immunoblotting.

For testing the direct interaction, His–Rab7bQ67L was incubated with GST or GST–myosin-II in PBS with 2 mM $MgCl_2$ and GTP 0.8 mM for 1 hour at 4℃ on a rotating wheel. Subsequently, pull down was performed using a glutathione resin. Samples were then subjected to SDS-PAGE and western blotting.

RhoA activity assay

RhoA activity was assessed by using a pulldown assay according to the manufacturer's instructions for a RhoA Activation Assay Biochem Kit (Cytoskeleton). Briefly, GTP-bound RhoA was immunoprecipitated from cell lysates with GST–Rhotekin-RBD bound to glutathione–agarose beads. After washing, the beads were subjected to western blot analysis using an anti-RhoA antibody to detect GTP-bound RhoA. Total proteins were detected by immunoblotting of whole cell lysates.

Cell spreading assay

Control cells and Rab7b-depleted cells (5×10^4 cells/ml) were seeded onto fibronectin-coated coverslips (10 µg/ml) and fixed 1 hour later. After

staining with Rhodamine-conjugated phalloidin, coverslips were mounted and examined using an Olympus FluoView FV1000 microscope. For real-time imaging of cell spreading, 5×10^4 cells/ml were seeded onto 10 µg/ml fibronectin-coated MatTek glass-bottomed dishes and imaged every 15 minutes at 37℃ under 5% CO_2. Live cells were imaged with a 40× PlanApo NA 0.90 objective on an Olympus Fluoview 1000 IX-81 inverted confocal laser scanning microscope. The cell area was determined by using ImageJ software (National Institutes of Health).

Cell migration assay

Wound-healing assays were performed by scratching confluent monolayers of HeLa cells with a pipette tip. Cells were imaged for a period of 24 hours with a 10× PlanApo NA 0.75 objective on a Scan^R imaging platform (Olympus) equipped with a Hamamatsu C8484-05G camera. Images were acquired every 3 hours using the Olympus Scan^R software. Cells were maintained in DMEM without phenol red at 37℃ under 5% CO_2 throughout the observation period. The velocity of migration was determined by using the Manual Tracking plugin of ImageJ software (National Institutes of Health) and the Chemotaxis and Migration Tool software (Ibidi).

Golgi reorientation measurements

A confluent monolayer of cells that had been cultured on glass slides was scratched with a pipette tip and incubated for 4 hours at 37℃ under 5% CO_2. Cells were fixed and stained with Rhodamine-conjugated phalloidin, Hoechst 33258 and anti-giantin antibody to visualize the actin cytoskeleton, the nuclei and Golgi, respectively. To measure Golgi reorientation, cells on the wound edge were equally divided into three sectors. The Golgi in the front sector between the nucleus and the leading edge was determined to be in the polarized position.

Immunofluorescence and live-cell microscopy

HeLa cells grown on coverslips were fixed with 3% paraformaldehyde, permeabilized with 0.25% saponin in PBS and incubated for 20 minutes at room temperature with primary antibodies. After washing with 0.25% saponin, coverslips were incubated with the appropriate secondary antibody for 20 minutes in the dark at room temperature. Mounted coverslips were examined by using a 63× PlanApo NA 1.42 objective on an Olympus FluoView FV1000 microscope with the FV1000 software (version 1.7a).

For live-imaging experiments, HeLa cells grown on MatTek glass-bottomed dishes were washed and incubated in DMEM without phenol red. Live cells were imaged with a 63× PlanApo NA 1.42 objective on an Olympus IX-71 microscope equipped with a CSU22 spinning-disk confocal unit (Yokogawa), an Ixon EMCCD camera (Andor) and the Andor iQ1.8 software. During imaging, cells were kept at 37℃ under 5% CO_2 in an incubation chamber (Solent Scientific).

Image analysis and processing

Image analysis and processing was performed using Adobe Photoshop (Adobe Systems) and ImageJ (National Institutes of Health).

Cell tracking was conducted using the Manual Tracking plugin of ImageJ software (National Institutes of Health). The speed of each migrating cell was calculated on the basis of the migration track by using the Chemotaxis and Migration Tool software (Ibidi GmbH). During each experiment, five videos were acquired for each condition, and a minimum number of 50 cells were analyzed per condition.

Object-based colocalization analysis was performed using ImageJ software to quantify the degree of colocalization between Rab7b vesicles and myosin II. Specifically, the number of Rab7b-positive vesicles with an overlapping signal from myosin II was measured with respect to the total number of Rab7b-positive vesicles within each cell.

Tracking of individual endosomes and quantification of velocity was performed using ImageJ Software using the Manual Tracking plugin. For each experiment, at least 30 different endosomes for each Rab protein were tracked manually for 1 minute, and the mean velocity was determined by the software.

Imaris Software (Bitplane AG) was used to analyze the length of endosomal movement during blebbistatin experiments. A representative area with regard to size and number of endosomes was chosen for each cell, and endosomal movement was tracked by the software for a 3-minute interval.

Statistical analysis

Statistical differences were assessed by using the one-tailed unpaired Student's *t*-test (GraphPad Prism4 software). In the figures, statistical significance is indicated as follows: $*P<0.05$, $**P<0.01$ and $***P<0.001$. Unless otherwise stated, data are from assays performed in triplicate, with error bars representing s.d. or s.e.m.

Acknowledgements

We thank Catherine Heyward, Gerbrand Koster and Frode Skjeldal (University of Oslo, Norway) for assistance with imaging and for comments on the manuscript. We also thank Ellen Haugsten and Jørgen Wesche (Oslo University Hospital, Norway) for useful advice on cell migration experiments. We are grateful to Gareth Griffiths (University of Oslo, Norway) and Harald Stenmark (Oslo University Hospital, Norway) for critically reading the manuscript.

Competing interests

The authors declare no competing interests.

Author contributions

C.P. conceived the project and designed experiments. M.B. and C.P. performed experiments and analyzed data. O.B. and C.P. supervised the project. M.B., O.B. and C.P. wrote the manuscript.

Funding

The research was supported by the Research Council of Norway [grant 197301 to C.P.] and through its Centres of Excellence funding scheme [project number 179573].

Supplementary material

Supplementary material available online at
http://jcs.biologists.org/lookup/suppl/doi:10.1242/jcs.155861/-/DC1

References

Aguilar-Cuenca, R., Juanes-García, A. and Vicente-Manzanares, M. (2014). Myosin II in mechanotransduction: master and commander of cell migration, morphogenesis, and cancer. *Cell. Mol. Life Sci.* **71**, 479-492.

Allaire, P. D., Seyed Sadr, M., Chaineau, M., Seyed Sadr, E., Konefal, S., Fotouhi, M., Maret, D., Ritter, B., Del Maestro, R. F. and McPherson, P. S. (2013). Interplay between Rab35 and Arf6 controls cargo recycling to coordinate cell adhesion and migration. *J. Cell Sci.* **126**, 722-731.

Amano, M., Ito, M., Kimura, K., Fukata, Y., Chihara, K., Nakano, T., Matsuura, Y. and Kaibuchi, K. (1996). Phosphorylation and activation of myosin by Rho-associated kinase (Rho-kinase). *J. Biol. Chem.* **271**, 20246-20249.

Amano, M., Chihara, K., Kimura, K., Fukata, Y., Nakamura, N., Matsuura, Y. and Kaibuchi, K. (1997). Formation of actin stress fibers and focal adhesions enhanced by Rho-kinase. *Science* **275**, 1308-1311.

Anitei, M. and Hoflack, B. (2012). Bridging membrane and cytoskeleton dynamics in the secretory and endocytic pathways. *Nat. Cell Biol.* **14**, 11-19.

Berg-Larsen, A., Landsverk, O. J. B., Progida, C., Gregers, T. F. and Bakke, O. (2013). Differential regulation of Rab GTPase expression in monocyte-derived dendritic cells upon lipopolysaccharide activation: a correlation to maturation-dependent functional properties. *PLoS ONE* **8**, e73538.

Bisel, B., Wang, Y., Wei, J.-H., Xiang, Y., Tang, D., Miron-Mendoza, M., Yoshimura, S., Nakamura, N. and Seemann, J. (2008). ERK regulates Golgi and centrosome orientation towards the leading edge through GRASP65. *J. Cell Biol.* **182**, 837-843.

Bresnick, A. R. (1999). Molecular mechanisms of nonmuscle myosin-II regulation. *Curr. Opin. Cell Biol.* **11**, 26-33.

Bucci, C., Thomsen, P., Nicoziani, P., McCarthy, J. and van Deurs, B. (2000). Rab7: a key to lysosome biogenesis. *Mol. Biol. Cell* **11**, 467-480.

Donaldson, J. G. and Jackson, C. L. (2011). ARF family G proteins and their regulators: roles in membrane transport, development and disease. *Nat. Rev. Mol. Cell Biol.* **12**, 362-375.

Goitre, L., Trapani, E., Trabalzini, L. and Retta, S. F. (2014). The Ras superfamily of small GTPases: the unlocked secrets. In *Ras Signaling: Methods and Protocols (Methods in Molecular Biology)*, Vol. 1120 (ed. L. Trabalzini and S. F. Retta), pp. 1-18. New York, NY: Humana Press.

Gomes, E. R., Jani, S. and Gundersen, G. G. (2005). Nuclear movement regulated by Cdc42, MRCK, myosin, and actin flow establishes MTOC polarization in migrating cells. *Cell* **121**, 451-463.

Hall, A. (2012). Rho family GTPases. *Biochem. Soc. Trans.* **40**, 1378-1382.

He, D., Chen, T., Yang, M., Zhu, X., Wang, C., Cao, X. and Cai, Z. (2011). Small Rab GTPase Rab7b promotes megakaryocytic differentiation by enhancing IL-6 production and STAT3-GATA-1 association. *J. Mol. Med.* **89**, 137-150.
Hirata, N., Takahashi, M. and Yazawa, M. (2009). Diphosphorylation of regulatory light chain of myosin IIA is responsible for proper cell spreading. *Biochem. Biophys. Res. Commun.* **381**, 682-687.
Hongu, T. and Kanaho, Y. (2014). Activation machinery of the small GTPase Arf6. *Advances in Biological Regulation* **54**, 59-66.
Horgan, C. P. and McCaffrey, M. W. (2011). Rab GTPases and microtubule motors. *Biochem. Soc. Trans.* **39**, 1202-1206.
Ikonen, E., de Almeid, J. B., Fath, K. R., Burgess, D. R., Ashman, K., Simons, K. and Stow, J. L. (1997). Myosin II is associated with Golgi membranes: identification of p200 as nonmuscle myosin II on Golgi-derived vesicles. *J. Cell Sci.* **110**, 2155-2164.
Katoh, K., Kano, Y., Amano, M., Kaibuchi, K. and Fujiwara, K. (2001a). Stress fiber organization regulated by MLCK and Rho-kinase in cultured human fibroblasts. *Am. J. Physiol.* **280**, C1669-C1679.
Katoh, K., Kano, Y., Amano, M., Onishi, H., Kaibuchi, K. and Fujiwara, K. (2001b). Rho-kinase – mediated contraction of isolated stress fibers. *J. Cell Biol.* **153**, 569-584.
Kawauchi, T., Sekine, K., Shikanai, M., Chihama, K., Tomita, K., Kubo, K., Nakajima, K., Nabeshima, Y. and Hoshino, M. (2010). Rab GTPases-dependent endocytic pathways regulate neuronal migration and maturation through N-cadherin trafficking. *Neuron* **67**, 588-602.
Kobayashi, H. and Fukuda, M. (2013). Arf6, Rab11 and transferrin receptor define distinct populations of recycling endosomes. *Commun. Integr. Biol.* **6**, e25036.
Kupfer, A., Louvard, D. and Singer, S. J. (1982). Polarization of the Golgi apparatus and the microtubule-organizing center in cultured fibroblasts at the edge of an experimental wound. *Proc. Natl. Acad. Sci. USA* **79**, 2603-2607.
Lewis-Saravalli, S., Campbell, S. and Claing, A. (2013). ARF1 controls Rac1 signaling to regulate migration of MDA-MB-231 invasive breast cancer cells. *Cell. Signal.* **25**, 1813-1819.
Lindsay, A. J., Jollivet, F., Horgan, C. P., Khan, A. R., Raposo, G., McCaffrey, M. W. and Goud, B. (2013). Identification and characterization of multiple novel Rab-myosin Va interactions. *Mol. Biol. Cell* **24**, 3420-3434.
Linford, A., Yoshimura, S., Nunes Bastos, R., Langemeyer, L., Gerondopoulos, A., Rigden, D. J. and Barr, F. A. (2012). Rab14 and its exchange factor FAM116 link endocytic recycling and adherens junction stability in migrating cells. *Dev. Cell* **22**, 952-966.
Mai, A., Veltel, S., Pellinen, T., Padzik, A., Coffey, E., Marjomäki, V. and Ivaska, J. (2011). Competitive binding of Rab21 and p120RasGAP to integrins regulates receptor traffic and migration. *J. Cell Biol.* **194**, 291-306.
Matsui, T., Amano, M., Yamamoto, T., Chihara, K., Nakafuku, M., Ito, M., Nakano, T., Okawa, K., Iwamatsu, A. and Kaibuchi, K. (1996). Rho-associated kinase, a novel serine/threonine kinase, as a putative target for small GTP binding protein Rho. *EMBO J.* **15**, 2208-2216.
Miserey-Lenkei, S., Chalancon, G., Bardin, S., Formstecher, E., Goud, B. and Echard, A. (2010). Rab and actomyosin-dependent fission of transport vesicles at the Golgi complex. *Nat. Cell Biol.* **12**, 645-654.
Morel, E., Parton, R. G. and Gruenberg, J. (2009). Annexin A2-dependent polymerization of actin mediates endosome biogenesis. *Dev. Cell* **16**, 445-457.
Myers, K. R. and Casanova, J. E. (2008). Regulation of actin cytoskeleton dynamics by Arf-family GTPases. *Trends Cell Biol.* **18**, 184-192.
Nakai, W., Kondo, Y., Saitoh, A., Naito, T., Nakayama, K. and Shin, H.-W. (2013). ARF1 and ARF4 regulate recycling endosomal morphology and retrograde transport from endosomes to the Golgi apparatus. *Mol. Biol. Cell* **24**, 2570-2581.
Naumanen, P., Lappalainen, P. and Hotulainen, P. (2008). Mechanisms of actin stress fibre assembly. *J. Microsc.* **231**, 446-454.
Parsons, J. T., Horwitz, A. R. and Schwartz, M. A. (2010). Cell adhesion: integrating cytoskeletal dynamics and cellular tension. *Nat. Rev. Mol. Cell Biol.* **11**, 633-643.
Progida, C., Malerød, L., Stuffers, S., Brech, A., Bucci, C. and Stenmark, H. (2007). RILP is required for the proper morphology and function of late endosomes. *J. Cell Sci.* **120**, 3729-3737.
Progida, C., Cogli, L., Piro, F., De Luca, A., Bakke, O. and Bucci, C. (2010). Rab7b controls trafficking from endosomes to the TGN. *J. Cell Sci.* **123**, 1480-1491.
Progida, C., Nielsen, M. S., Koster, G., Bucci, C. and Bakke, O. (2012). Dynamics of Rab7b-dependent transport of sorting receptors. *Traffic* **13**, 1273-1285.
Riento, K. and Ridley, A. J. (2003). Rocks: multifunctional kinases in cell behaviour. *Nat. Rev. Mol. Cell Biol.* **4**, 446-456.
Roland, J. T., Bryant, D. M., Datta, A., Itzen, A., Mostov, K. E. and Goldenring, J. R. (2011). Rab GTPase-Myo5B complexes control membrane recycling and epithelial polarization. *Proc. Natl. Acad. Sci. USA* **108**, 2789-2794.
Rottner, K. and Stradal, T. E. B. (2011). Actin dynamics and turnover in cell motility. *Curr. Opin. Cell Biol.* **23**, 569-578.
Schlienger, S., Campbell, S. and Claing, A. (2014). ARF1 regulates the Rho/MLC pathway to control EGF-dependent breast cancer cell invasion. *Mol. Biol. Cell* **25**, 17-29.
Seabra, M. C. and Coudrier, E. (2004). Rab GTPases and myosin motors in organelle motility. *Traffic* **5**, 393-399.
Shutova, M., Yang, C., Vasiliev, J. M. and Svitkina, T. (2012). Functions of nonmuscle myosin II in assembly of the cellular contractile system. *PLoS ONE* **7**, e40814.
Spinosa, M. R., Progida, C., De Luca, A., Colucci, A. M. R., Alifano, P. and Bucci, C. (2008). Functional characterization of Rab7 mutant proteins associated with Charcot-Marie-Tooth type 2B disease. *J. Neurosci.* **28**, 1640-1648.
Stenmark, H. (2009). Rab GTPases as coordinators of vesicle traffic. *Nat. Rev. Mol. Cell Biol.* **10**, 513-525.
Tsai, J.-C., Lin, Y.-W., Huang, C.-Y., Lin, C.-Y., Tsai, Y.-T., Shih, C.-M., Lee, C.-Y., Chen, Y.-H., Li, C.-Y., Chang, N.-C. et al. (2014). The role of calpain-myosin 9-Rab7b pathway in mediating the expression of Toll-like receptor 4 in platelets: a novel mechanism involved in α-granules trafficking. *PLoS ONE* **9**, e85833.
Wang, Y., Chen, T., Han, C., He, D., Liu, H., An, H., Cai, Z. and Cao, X. (2007). Lysosome-associated small Rab GTPase Rab7b negatively regulates TLR4 signaling in macrophages by promoting lysosomal degradation of TLR4. *Blood* **110**, 962-971.
Wang, H. H., Tanaka, H., Qin, X., Zhao, T., Ye, L.-H., Okagaki, T., Katayama, T., Nakamura, A., Ishikawa, R., Thatcher, S. E. et al. (2008). Blebbistatin inhibits the chemotaxis of vascular smooth muscle cells by disrupting the myosin II-actin interaction. *Am. J. Physiol.* **294**, H2060-H2068.
Watanabe, T., Hosoya, H. and Yonemura, S. (2007). Regulation of myosin II dynamics by phosphorylation and dephosphorylation of its light chain in epithelial cells. *Mol. Biol. Cell* **18**, 605-616.
Wei, Q. and Adelstein, R. S. (2000). Conditional expression of a truncated fragment of nonmuscle myosin II-A alters cell shape but not cytokinesis in HeLa cells. *Mol. Biol. Cell* **11**, 3617-3627.
Wiesner, C., El Azzouzi, K. and Linder, S. (2013). A specific subset of RabGTPases controls cell surface exposure of MT1-MMP, extracellular matrix degradation and three-dimensional invasion of macrophages. *J. Cell Sci.* **126**, 2820-2833.
Worthylake, R. A. and Burridge, K. (2003). RhoA and ROCK promote migration by limiting membrane protrusions. *J. Biol. Chem.* **278**, 13578-13584.
Yang, M., Chen, T., Han, C., Li, N., Wan, T. and Cao, X. (2004). Rab7b, a novel lysosome-associated small GTPase, is involved in monocytic differentiation of human acute promyelocytic leukemia cells. *Biochem. Biophys. Res. Commun.* **318**, 792-799.
Yao, M., Liu, X., Li, D., Chen, T., Cai, Z. and Cao, X. (2009). Late endosome/lysosome-localized Rab7b suppresses TLR9-initiated proinflammatory cytokine and type I IFN production in macrophages. *J. Immunol. (Baltimore, MD)* **183**, 1751-1758.

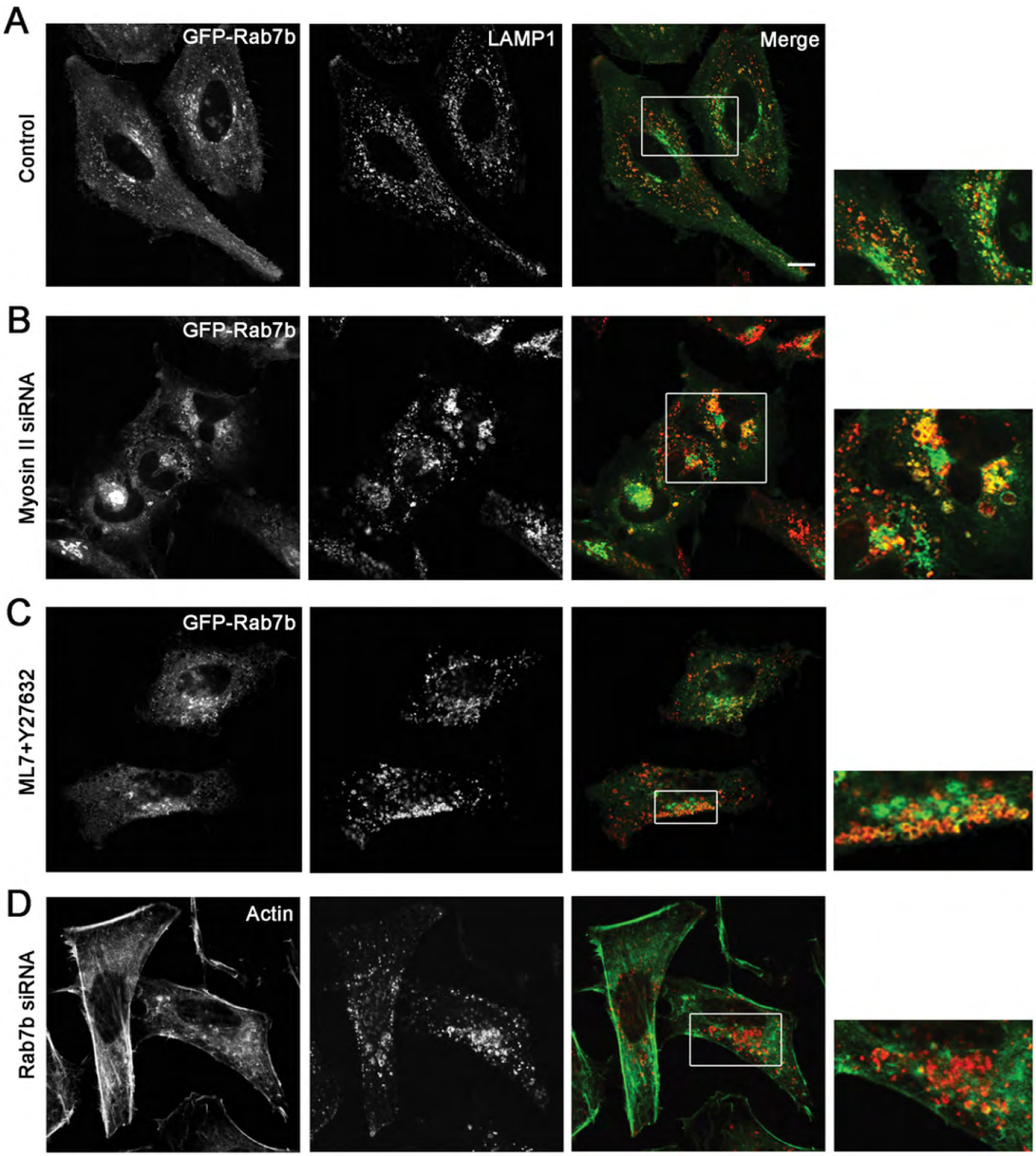

Figure S1: Inhibition of myosin II causes enlargement of Rab7b-positive late endosomes.

Cells transfected with GFP-Rab7b **(A)** and depleted for myosin II **(B)** or incubated 40 minutes with 30 μM ML7 and 10 μM Y27632 **(C)** were fixed and stained with anti-Lamp-1 antibody. Cells silenced for Rab7b were fixed and stained with anti-Lamp-1 antibody and phalloidin **(D)**. Scale bar, 10 μM. In the insets, magnifications of the boxed areas show late endosomes.

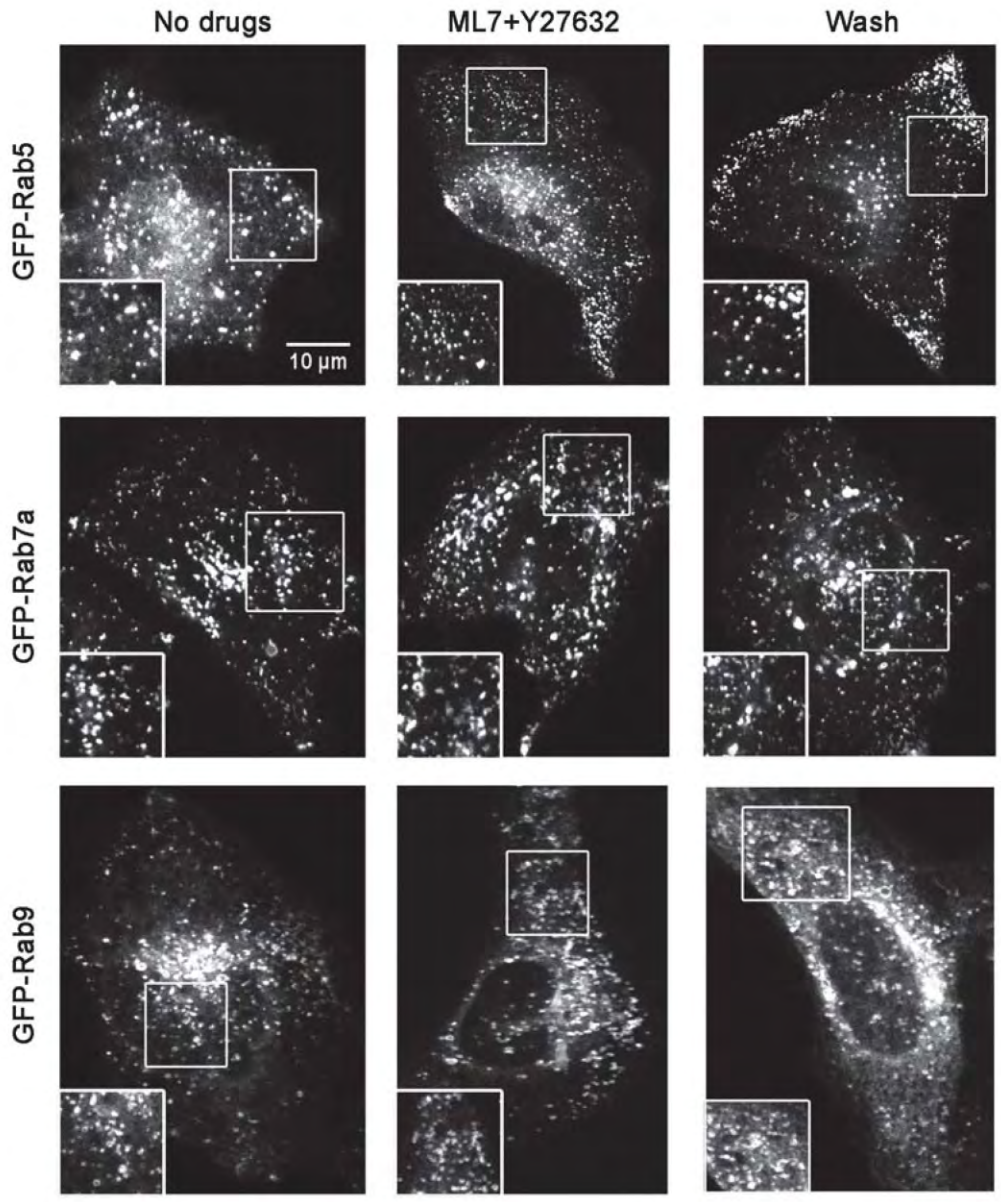

Figure S2: The inhibitory mix ML7+Y27632 has no effect on Rab5, Rab7a or Rab9 endosomes.

HeLa cells were transfected with GFP-Rab5, GFP-Rab7a, or GFP-Rab9, and imaged using a Spinning Disk confocal microscope at 37° C with 5% CO_2. Imaging was done before addition of the inhibitor mix ML7+Y27632 (no drugs), 40 minutes after addition of 30 µM ML7 and 10 µM Y27632, and after washing away the inhibitory drugs (after wash). Scale bar, 10 µm.

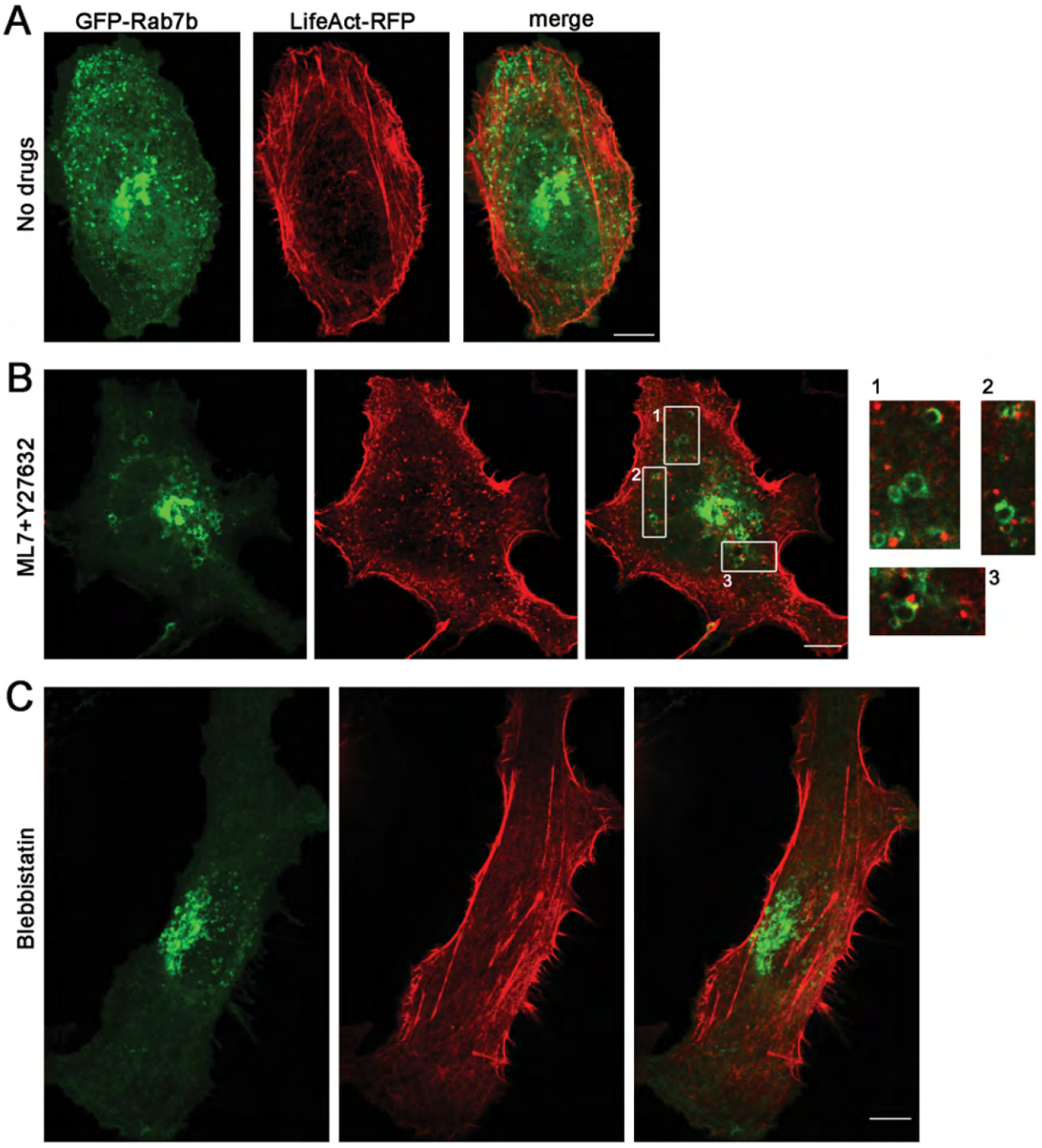

Figure S3: Myosin II inhibitors affect differently actin cytoskeleton.

HeLa cells co-transfected with GFP-Rab7b and LifeAct-RFP were imaged using a Spinning Disk confocal microscope before addition of chemical inhibitors **(A)**, after 40 minutes of incubation with 30 µM ML7 and 10 µM Y27632 **(B)**, or 40 minutes after addition of blebbistatin (25 µM), **(C)**. Scale bars, 10 µM. In the insets, magnifications of the boxed areas show actin puncta on Rab7b positive-endosomes.

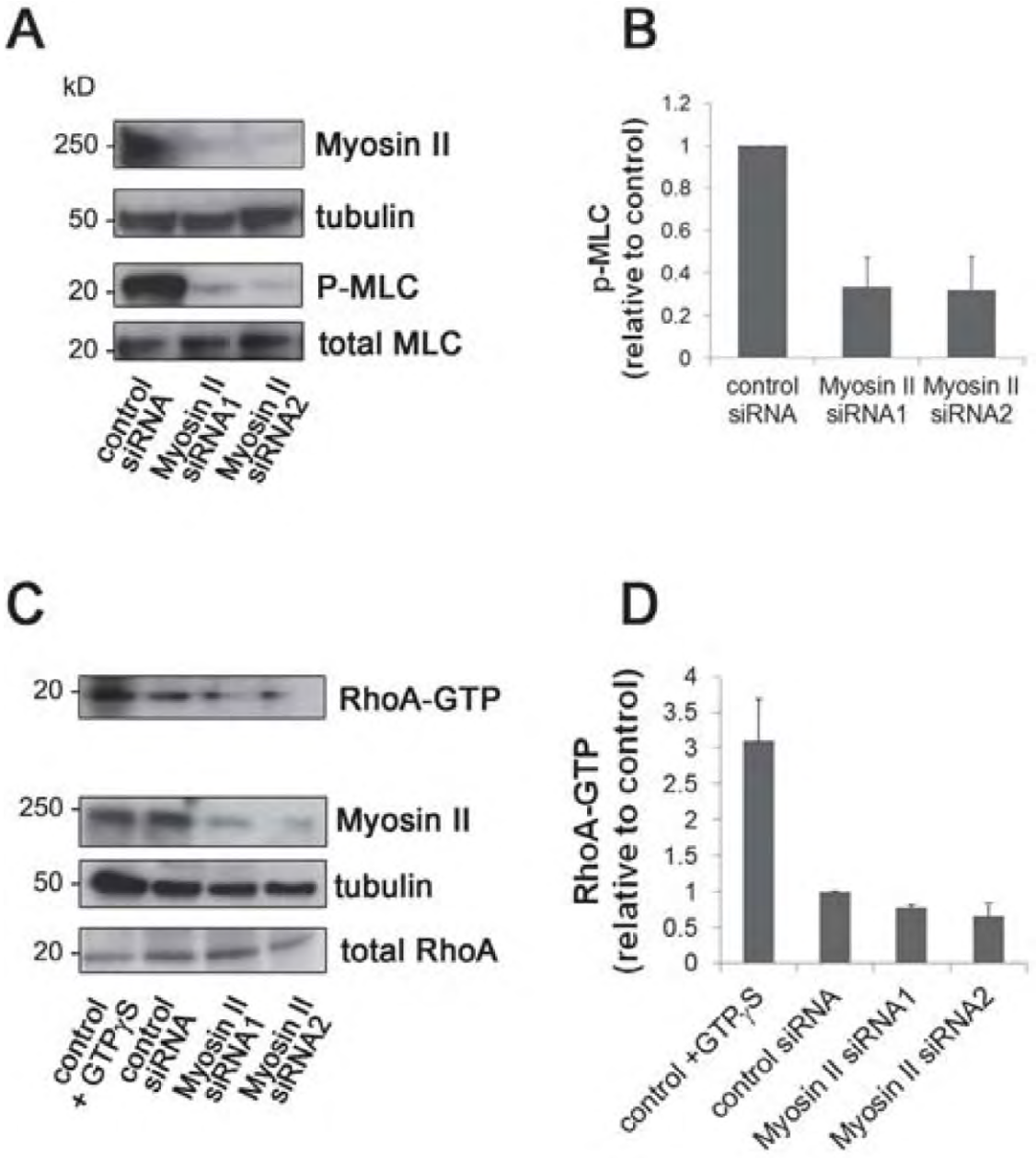

Figure S4. Effects on MLC phosphorylation and RhoA activity after myosin II depletion.

A Lysates from HeLa cells transfected with either control siRNA or or two different siRNAs against myosin II were subjected to western blot analysis using antibodies against myosin II, phosphorylated myosin light chain (P-MLC), total MLC, and tubulin (as a loading control).

B Quantification of P-MLC levels in control and myosin II-depleted cells. The intensities of the bands from the western blot were normalized to the amount of tubulin and plotted relative to the intensities of P-MLC in the control siRNA sample. Quantifications are based on three independent experiments and were determined using ImageQuant Software (Amersham). Error bars represent ± s.e.m.

C Lysates from HeLa cells transfected with either control siRNA or or two different siRNAs against myosin II, were mixed with GST–Rhotekin–RBD bound to glutathion-agarose beads to precipitate the active form (GTP-bound) of RhoA. As a positive control, cells were loaded with GTPγS. The immunoprecipitate samples were subjected to western blot analysis using antibodies against RhoA, myosin II, and tubulin (loading control).

D Quantification of the levels of active RhoA in control and myosin II-depleted cells. Intensities of the bands from the western blot were quantified with ImageQuant, normalized to the amount of tubulin and plotted relative to the intensities of GTP-bound RhoA in the control sample. The values represent the mean ± s.e.m. of 5 independent experiments.

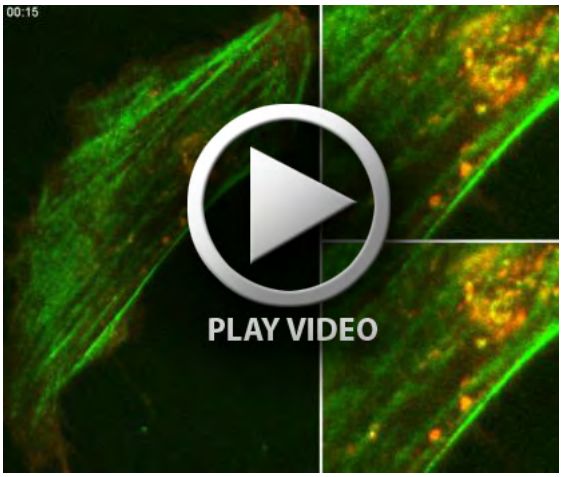

Movie1: Rab7b and myosin II colocalize and move together. HeLa cells co-transfected with GFP-myosin II (green) and mCherry-Rab7b (red) were imaged with a Spinning Disk confocal microscope at 1 second intervals. In the enlarged area is visible a vesicle positive for both GFP-myosin II and mCherry-Rab7b moving toward the Golgi region and the tracking of the same vesicle over time.

Movie2: Depletion of myosin II results in clustering and enlargement of Rab7b-positive endosomes. HeLa cells were transfected with either the control siRNA (left) or with two different siRNAs (mid, right) targeted against myosin II, and further transfected with GFP-Rab7b. The cells were imaged using a Spinning Disk confocal microscope at 1 second intervals.

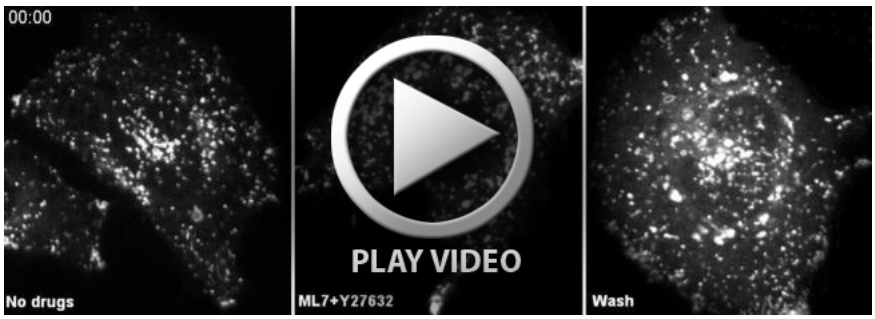

Movie3: ML7 and Y27632 do not affect Rab7a-positive endosomes. HeLa cells transiently transfected with GFP-Rab7a were imaged using a Spinning Disk confocal microscope at 1 second intervals before adding the drug (left), 40 minutes after the addition of 30 μM ML7 and 10 μM Y27632 (mid), and after washing away the inhibitory drugs (right).

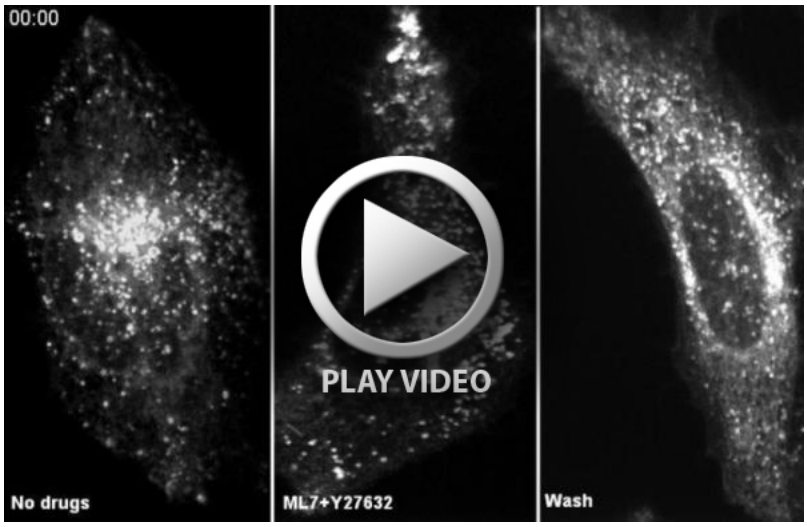

Movie4: ML7 and Y27632 do not affect Rab9-positive endosomes. HeLa cells transiently transfected with GFP-Rab9 were imaged using a Spinning Disk confocal microscope at 1 second intervals before adding the drug (left), 40 minutes after the addition of 30 µM ML7 and 10 µM Y27632 (mid), and after washing away the inhibitory drugs (right).

Movie5: ML7 and Y27632 affect size, distribution and velocity of Rab7b-positive endosomes. HeLa cells transiently transfected with GFP-Rab7b were imaged using a Spinning Disk confocal microscope at 1 second intervals before adding the drug (left), 40 minutes after the addition of 30 µM ML7 and 10 µM Y27632 (mid), and after washing away the inhibitory drugs (right).

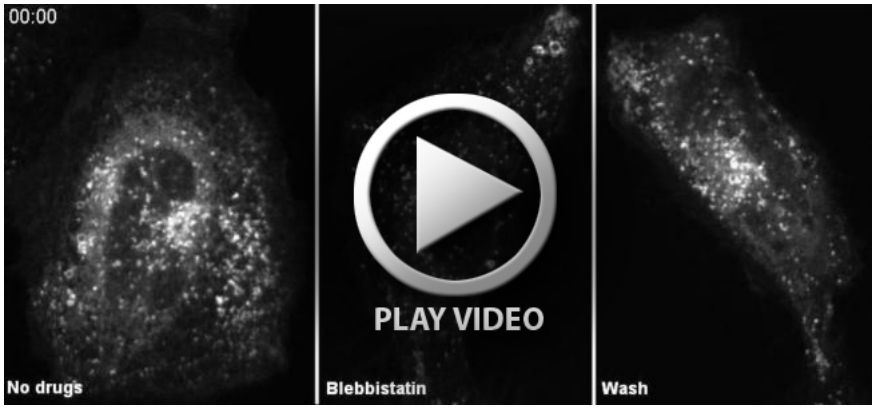

Movie6: Blebbistatin does not affect Rab9-positive endosomes. HeLa cells transiently transfected with GFP-Rab9 were imaged using a Spinning Disk confocal microscope at 1 second intervals before adding the drug (left), 40 minutes after the addition of 25 µM blebbistatin (mid), and after washing away the inhibitory drugs (right).

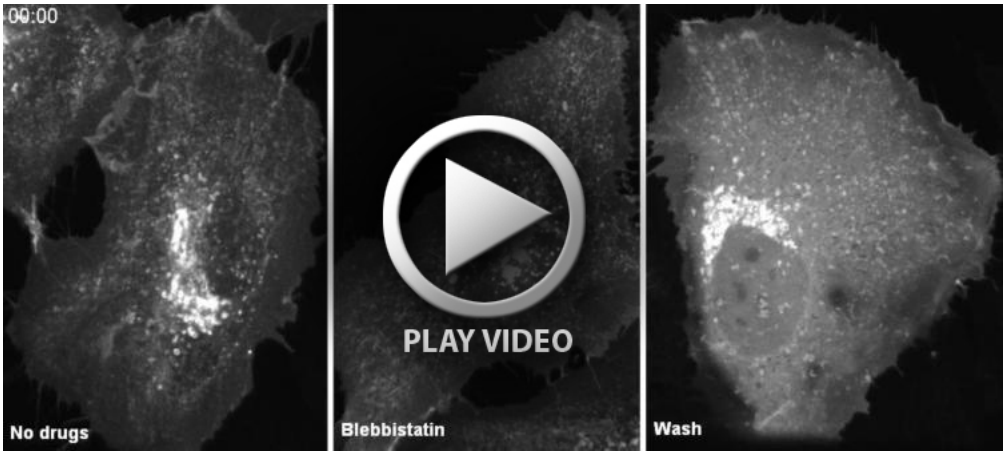

Movie7: Blebbistatin decreases the velocity of Rab7b-positive endosomes. HeLa cells transiently transfected with GFP-Rab7b were imaged using a Spinning Disk confocal microscope at 1 second intervals before adding the drug (left), 40 minutes after the addition of 25 μM blebbistatin (mid), and after washing away the inhibitory drugs (right).

Movie 8: Rab7b knockdown affects cell spreading. HeLa cells transfected with either control siRNA (left) or with siRNA targeting Rab7b (right) were plated on fibronectin-coated dishes and cell spreading was imaged by an Olympus Fluoview 1000 IX81 inverted confocal laser scanning microscope every 15 minutes.

Movie9: Depletion of Rab7b delays wound closure. Confluent HeLa cells transfected with either control siRNA (top) or with siRNA targeting Rab7b (bottom) were wounded and the migration of the cells towards the wound area was imaged by a Scanˆ R imaging platform (Olympus) every 3 hours.